 Bull. Chem. Soc. Jpn. Vol. 81, No. 9, 1131–1146 (2008)

Crystal Structures, Degree of Charge Transfer, and Non-Linear Optical Characteristics of Intramolecular Charge-Transfer Compounds: Indoline-Substituted Tricyanoquinodimethanes[1]

Tsuyoshi Murata,*[1] Gunzi Saito,*[1,2,3] Kazukuni Nishimura,[1] Chin-Hong Chong,[1] Masaru Makihara,[1] Genki Honda,[1] Yuichiro Enomoto,[1] Salavat Khasanov,[1,4] Hideki Yamochi,[2] Akihiro Otsuka,[2] Kenji Kamada,[5] Koji Ohta,[5] and Jun Kawamata[6]

[1]Division of Chemistry, Graduate School of Science, Kyoto University, Sakyo-ku, Kyoto 606-8502

[2]Research Center for Low Temperature and Materials Sciences, Kyoto University, Sakyo-ku, Kyoto 606-8502

[3]Research Institute, Meijo University, Tenpaku-ku, Nagoya 468-8502

[4]The Institute of Solid State Physics of Russian Academy of Science, Chernogolovka 142432, Russia

[5]Photonics Research Institute, National Institute of Advanced Industrial Science and Technology (AIST), AIST Kansai Center, Ikeda, Osaka 563-8577

[6]Department of Chemistry, Faculty of Science, Yamaguchi University, Yamaguchi 753-8512

Received March 14, 2008; E-mail: saito@kuchem.kyoto-u.ac.jp

The substituent effect on the degree of intramolecular charge transfer (δ) and optical properties of donor–π–acceptor compounds comprised of 1,3,3-trimethyl-2-methyleneindoline ($\mathbf{I}_1$) and substituted 7,8,8-tricyanoquinodimethane (=2-(4-cyanomethylene-2,5-cyclohexadienylidene)malononitrile, 3CNQ-R, R = substituent groups) moieties were investigated ($\mathbf{I}_1$–3CNQ-R). In the crystal structures, $\mathbf{I}_1$–3CNQ-R molecules stacked on indoline and/or 3CNQ-R moieties in a head-to-tail manner to cancel their dipole moments and established segregated or mixed stack columnar motifs. The δ values of $\mathbf{I}_1$–3CNQ-R molecules in solid and solution states were estimated using the bond length ratio in the crystal structures, molecular orbital calculation, and the solvatochromic shift of intramolecular charge-transfer absorption, respectively, and showed significant and reasonable dependences on substituents of the 3CNQ moiety. Structural analysis revealed that molecular conformation and planarity affect the δ values of $\mathbf{I}_1$–3CNQ-R molecules. Molecular orbital calculations revealed that molecular (hyper)polarizabilities can be modulated by tuning δ. $\mathbf{I}_1$–3CNQ-R exhibited a solvatochromic shift, and the ground state changed from neutral ($\delta \leq 0.5$) in less-polar solvents to ionic ($\delta \geq 0.5$) in polar solvents. Two-photon absorption properties of $\mathbf{I}_1$–3CNQ-R showed a significant substituent effect and indicated that δ is a fundamental parameter for modulating non-linear optical properties.

Since the first proposal in 1974 of a tetrathiafulvalene (=2-(1,3-dithiol-2-ylidene)-1,3-dithiole, TTF)–tetracyanoquinodimethane (=3,6-bis(dicyanomethylene)-1,4-cyclohexadiene, TCNQ) compound linked through a covalent bond by Aviram and Ratner,[2] many scientists studying functional molecular materials have been exploring numerous unimolecular donor (D)–acceptor (A) compounds.[3,4] Intramolecular charge-transfer (CT) compounds, $D^{\delta+}$–π–$A^{\delta-}$ (δ = degree of CT), where D and A moieties are linked by a π-bond, have a flexible electronic structure, amphoteric redox ability, and large dipole moment. These features of $D^{\delta+}$–π–$A^{\delta-}$ are interesting for use in molecular optics and electronics such as indicators of solvent polarity,[5,6] molecular rectifiers,[4,7–10] organic field-effect transistors,[11] non-linear optics,[12–23] photovoltaics,[24] photochromic materials,[12,25] organic conductors,[26,27] and molecular magnets.[28,29] The reaction between amine derivatives (alkylamines, *N*-alkyl picolinium, lepidinium, benzothiazolium, etc.) and strong π-acceptor molecules (TCNQ,[7,14,30] tetracyanoethylene,[18,31] and *p*-chloranil[32]) yields stable $D^{\delta+}$–π–$A^{\delta-}$ compounds, which have been studied as various organic functional materials. Among these $D^{\delta+}$–π–$A^{\delta-}$ systems, donor–tricyanoquinodimethane (=2-(4-cyanomethylene-2,5-cyclohexadienylidene)malononitrile, 3CNQ), D–3CNQ, derivatives have been studied most intensively.[4,6–14,25,30]

For binary intermolecular CT complexes composed of electron-donor and -acceptor molecules, the degree of CT is one of the most important parameters governing their properties and functions such as conductivity[33–35] and phase transitions (neutral–ionic (N–I), Mott, Peierls, charge order, etc.).[36–38] In particular, to afford highly conducting CT complexes or N–I phase-transition systems, the selection of D and A moieties having appropriate donor and acceptor strengths is one of the most important strategies.[34–36] In the case of $D^{\delta+}$–π–$A^{\delta-}$ compounds, the degree of intramolecular CT (δ), which indicates the charge distribution in a molecule, is an important parameter governing their (hyper)polarizabilities and nonlinear optical properties.[14–16] Therefore, the control and estimation of the δ value are indispensable in molecular design.

Several D–tetrafluoro-substituted 3CNQ (3CNQ-F_4) derivatives have been prepared;[6,9,25a] however, modulation of the δ

Published on the web September 11, 2008; doi:10.1246/bcsj.81.1131

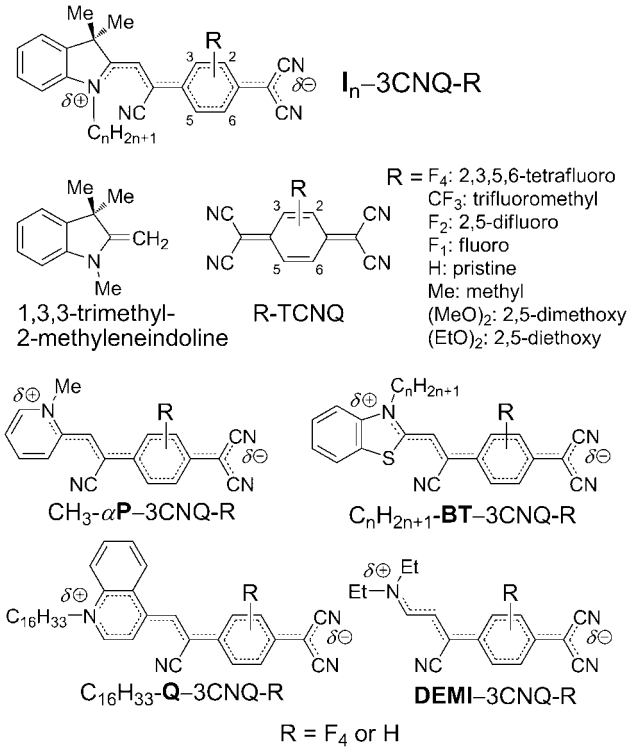

Chart 1. Chemicals discussed in this study.

value by systematic chemical modifications has not been reported for the D–3CNQ system. In addition, estimation of the δ value, which is necessary to understand the properties of a $D^{\delta+}$–π–$A^{\delta-}$ molecule, has rarely been demonstrated. Broo and Zerner demonstrated the theoretical calculation of CH_3-αP–3CNQ (αP = α-picolinium) and deduced the δ value from the sums of atomic charges on both D and A moieties.[39] Bell et al. assumed an ionic ground state for C_nH_{2n+1}-BT–3CNQ (BT = benzothiazolium) based on their solvatochromic shifts, although quantitative estimation was not performed.[6] For several other cases, completely neutral or ionic states (δ = 0 or 1) have been anticipated.[4a,8,14,17,18,40–42]

We have been studying a series of $D^{\delta+}$–π–$A^{\delta-}$ compounds, *N*-alkyl indoline–3CNQ derivatives ($\mathbf{I}_n$–3CNQ-R, Chart 1, n = *N*-alkyl chain length and R = substituent groups on the 3CNQ moiety) prepared by the Stork-enamine reaction between 1-alkyl-3,3-dimethyl-2-methyleneindoline and R-TCNQ.[1,43,44] In our previous study, crystal structure analyses of $\mathbf{I}_n$–3CNQ-H derivatives with various lengths of alkyl chains (R = H and n = 2–20) revealed that bond length ratio (*BLR*, vide infra) shows a good linear relationship with the δ value and that the molecular conformation (Type I and II, vide infra) has a notable effect on the δ value.[43] In the present study, to elucidate the effects of chemical modification on the electronic structure (δ value) and properties of $\mathbf{I}_n$–3CNQ-R compounds, we have systematically prepared $\mathbf{I}_1$–3CNQ-R derivatives with various substituent groups (R = F_4, CF_3, F_2, F_1, H, Me, $(MeO)_2$, and $(EtO)_2$). Here, we report the crystal structures and estimations of the δ values based on the *BLR* in the crystal structures and solvatochromic shift of the intramolecular CT absorption band. We also discuss molecular (hyper)polarizabilities and two-photon absorption properties in connection with the δ value.

Experimental

Measurements and Calculations. ^{1}H NMR spectra were measured at 400 MHz on a JEOL JNM-FX400 spectrometer using $CDCl_3$ or DMSO-d_6 as a solvent and tetramethylsilane as an internal standard. Elemental analyses were performed at the Center for Organic Elemental Microanalysis, Kyoto University. Melting points were measured with a Yanaco MP-500D micro melting-point apparatus and were not corrected. Ultraviolet–visible (UV–vis) spectra were measured on a Shimadzu UV-3100 spectrometer. Infrared (IR) spectra of the samples in KBr pellets were measured using a Perkin-Elmer PARAGON 1000 Series FT-IR spectrometer (resolution 2 or 4 cm^{-1}). Semi-empirical molecular orbital (MO) calculations were performed using MOS/F V4 with INDO/S parameterization coupled with a 20-dimensional CI matrix, which is sufficient to obtain approximately invariant dipole moments. Geometrical parameters were extracted from the crystal structures. Two-photon absorption cross-sections ($\sigma^{(2)}$) were estimated by the *Z*-scan technique[45] employing femtosecond laser pulses emitted from an optical parametric amplifier (OPA, SpectraPhysics OPA-800) pumped by a Ti–sapphire regenerative amplifier system (SpectraPhysics Spitfire, Merlin, Tsunami, and Millennia). The typical energy and pulse width used for the measurements were 1 μJ and 100 fs, respectively. Non-linear absorption behavior was observed with an ordinary optical configuration of an open aperture *Z*-scan method.[45] Laser pulses were nearly Gaussian in time and space as confirmed by beam profile and autocorrelation measurements, respectively.[46] Reliable results were obtained for a concentrated solution. To maximize the concentrations, acetonitrile (MeCN) and $CHCl_3$ were used as the solvents for R = CF_3, F_2, and F_1 and R = H, Me, $(MeO)_2$, and $(EtO)_2$, respectively. The recorded traces were fit with the theoretical equation for normalized transmittance through a pure two-photon absorption medium.

$$T_N(\zeta) = \frac{(1-R)^2}{\sqrt{\pi}q(\zeta)}\int_{-\infty}^{\infty}\ln[1+q(\zeta)\exp(-x^2)]dx \quad (1)$$

with $q(\zeta) = q_0/(1+\zeta^2)$. Here, T_N denotes the normalized transmittance as a function of normalized *z*-position $\zeta = (z - z_0)/z_R$ with the position of the beam waist z_0. *R* is the Fresnel reflectance at the cell wall. The linear absorption can be neglected at the wavelength of measurement. Curve fitting with eq 1 provides the two-photon absorption parameter q_0, defined as

$$q_0 = \alpha^{(2)}(1-R)I_0L \quad (2)$$

where $\alpha^{(2)}$, I_0, and L are the two-photon absorption coefficient, on-axis peak intensity of the incident pulse (calculated for every set of *Z*-scan measurements), and sample length. The power range was selected by confirming the linearity between q_0 and incident power to exclude the effect of other processes such as three-photon absorption and excited state absorption. From the $\alpha^{(2)}$ value obtained from the slope of the plot between q_0 and incident power, the two-photon cross-section $\sigma^{(2)}$ was calculated with the equation

$$\sigma^{(2)} = \frac{\hbar\omega\alpha^{(2)}}{N} \quad (3)$$

where $\hbar\omega$ is the energy of the incident photon and N is the number density of solute molecules.[47]

Preparation of $\mathbf{I}_1$–3CNQ-R. $\mathbf{I}_1$–3CNQ-R derivatives were prepared by the methods used for preparing 3CNQ-type $D^{\delta+}$–π–$A^{\delta-}$ systems:[6,7,12,25a] 1,3,3-Trimethyl-2-methyleneindoline (**I**) (1 mol equiv) and R-TCNQ (1 mol equiv) were reacted in dry

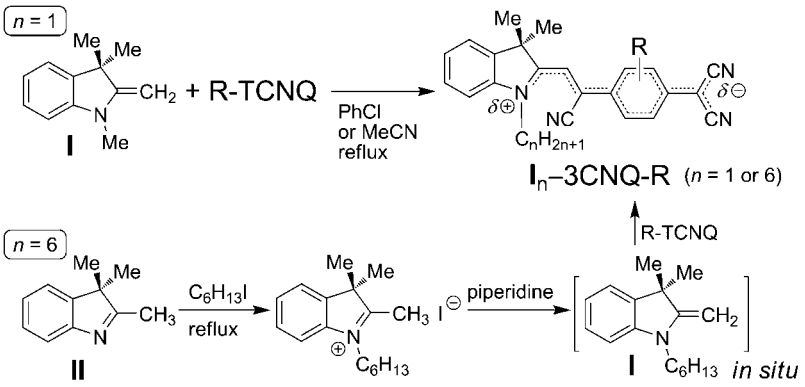

Scheme 1. Synthetic procedures for $\mathbf{I}_n$–3CNQ-R.

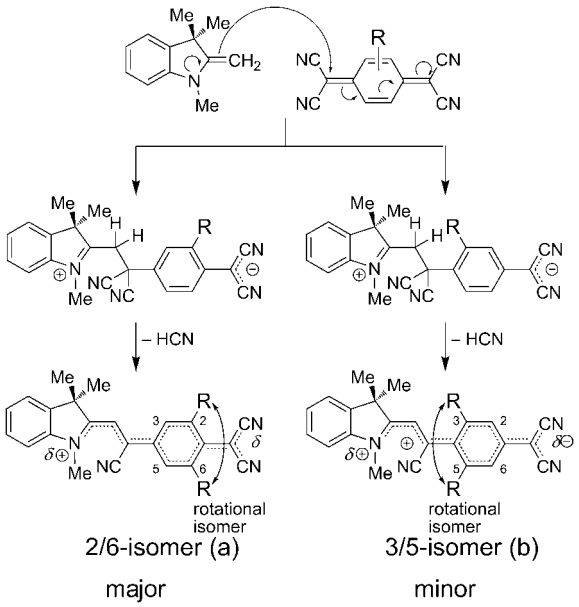

Scheme 2. Reaction mechanism to produce 2/6- and 3/5-isomers (denoted (a) and (b), respectively) of mono-substituted $\mathbf{I}_1$–3CNQ-R derivatives.

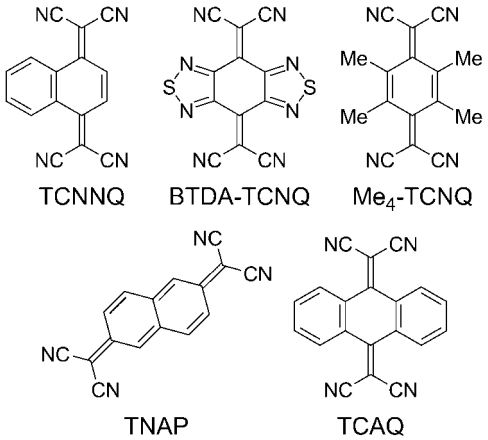

Chart 2. π-Extended or bulky TCNQ derivatives which did not yield $D^{\delta+}$–π–$A^{\delta-}$.

chlorobenzene (PhCl) under reflux (Scheme 1). $\mathbf{I}_6$–3CNQ-CF_3 was prepared by the reaction of CF_3-TCNQ and 1-hexyl-3,3-dimethyl-2-methyleneindoline, which was generated in situ in two steps from 2,3,3-trimethyl-3*H*-indole (**II**). Stork-enamine reaction of mono-substituted R-TCNQ derivatives (R = Me, F_1, and CF_3) is expected to yield 2/6- and 3/5-isomers (denoted as a and b in Scheme 2) related to substituent positions on the 3CNQ moiety, where 2/6- and 3/5-indicate the rotational isomers. All mono-substituted R-TCNQ afforded the 2/6-isomers as major products. The 3/5-isomer was obtained only for R = F_1 as the minor product (a:b $\geq$ 10:1 from the ^{1}H NMR spectra of the reaction mixture), and those of R = Me and CF_3 derivatives were not obtained. The steric repulsion of substituent groups would be the origin of the selectivity in products. In the intermediate generated by the nucleophilic addition of the methylene group of **I** to the dicyanomethylene group of R-TCNQ, the steric repulsion around the 3/5-substituent group is larger than that of the 2/6-substituent group, resulting in the selective formation of the 2/6-isomer (Scheme 2).

The reactions of **I** with π-extended or bulky TCNQ derivatives (Chart 2): tetracyano-1,4-naphthoquinodimethane (TCNNQ, reduction potential (E^A) = +0.07 V vs. SCE), tetracyano-2,6-naphthoquinodimethane (TNAP, +0.26 V), bis(1,2,5-thiadiazolo)-TCNQ (BTDA-TCNQ, +0.03 V), 2,3,5,6-tetramethyl-TCNQ (Me_4TCNQ, −0.05 V), and tetracyano-9,10-anthraquinodimethane (TCAQ, −0.32 V) did not afford $D^{\delta+}$–π–$A^{\delta-}$ type products.

Typical Procedure for Preparation: $\mathbf{I}_1$–3CNQ-F_2. F_2-TCNQ (480 mg, 2.00 mmol) was dissolved in PhCl (30 mL) under reflux. **I** (0.35 mL, 1.98 mmol) in PhCl (30 mL) was added dropwise, and the reaction mixture was refluxed for 5 h under nitrogen atmosphere. The resulting green solution was cooled to room temperature and filtered to yield the product. The resulting crude product was recrystallized from MeCN to yield ($\mathbf{I}_1$–3CNQ-F_2)$(MeCN)_{0.5}$ (150 mg, 18%) as black rod crystals. Physical data for the characterization are summarized in Supporting Information.

X-ray Crystal Structure Analyses. The intensity data of structural analyses were collected using a Bruker AXS DIP-2020K oscillator type X-ray imaging plate or MAC Science MXC^X automatic four-circle diffractometer with monochromated Mo Kα (λ = 0.71073 Å, 1 Å = 0.1 nm) radiation. Structures were determined by a direct method using SHELXS-97.[48] Least-squares refinements were performed by the full-matrix least-squares method on F^2 with SHELXL-97.[49] All non-hydrogen atoms were refined anisotropically. Hydrogen atoms were included without refinement. Positions of the hydrogen atoms were calculated assuming sp^3 or sp^2 conformations of carbon atoms. Crystallographic data have been deposited with the Cambridge Crystallographic Data Centre: Deposition numbers CCDC-686454–

686463. Copies of the data can be obtained free of charge via http://www.ccdc.cam.ac.uk/conts/retrieving.html (or from the Cambridge Crystallographic Data Centre, 12, Union Road, Cambridge, CB2 1EZ, UK; Fax: +44 1223 336033; e-mail: deposit@ccdc.cam.ac.uk). Crystallographic data are summarized in Supporting Information.

Results and Discussion

Molecular and Crystal Structures. Recrystallization of $\mathbf{I}_1$–3CNQ-R (R = F_4 (**A**), F_2 (**C**), F_1 (**D**), $(MeO)_2$ (**E**), and $(EtO)_2$ (**F**)) from MeCN yielded single crystals suitable for X-ray crystal structure analysis. Crystals of $\mathbf{I}_6$–3CNQ-CF_3 (**B**) were obtained from methanol (MeOH). In the cases of R = F_1, $(MeO)_2$, and $(EtO)_2$ derivatives, two or three kinds of polymorphs (labeled as **a**–**c**) were obtained. Polymorphs of $\mathbf{I}_1$–3CNQ-F_1 contained different kinds of isomers concerning the position of the fluorine atom on the 3CNQ moiety, 2/6-F ($\mathbf{I}_1$–3CNQ-F_1a, disordered) (**Da**) and 3-F isomers ($\mathbf{I}_1$–3CNQ-F_1b, **Db** and **Dc**) (Scheme 2), respectively, the former of which included the 3-F isomer as a minor impurity (8–9%). In the crystal structures, the indoline–indoline and/or 3CNQ–3CNQ π-stacking structures in a head-to-tail manner to cancel molecular dipole moments were the most common, and constructed one-dimensional segregated or mixed stacking structures. Due to the formation of centrosymmetric π-stacking motifs, second-order non-linear optical properties such as second-harmonic generation which need the alignment of the dipole moments to form non-centrosymmetric systems are not expected for their bulk crystals. Although several compounds had segregated stacking structures of the indoline and 3CNQ-R moieties, they were electrically insulators because they did not have radical electrons as conduction carrier.

In the crystal structures, two molecular conformations, Type I and II, were observed in which the *N*-alkyl group is located close to and far from the CN1 group, respectively (Scheme 3). The dihedral angle (θ_3) between the indoline moiety and the cyanoethene π-bridge distinguishes Type I ($\theta_3 < 90°$) and II ($\theta_3 > 90°$). Dihedral angle between the benzenoid ring in the 3CNQ moiety and the terminal dicyanomethylene group is indicated by θ_1 and that between the ring and the cyanoethene π-bridge by θ_2. The molecular conformations and dihedral angles (θ_1–θ_3) of the D and A parts are summarized in Table 1.

$\mathbf{I}_1$–3CNQ-F_4 (A): Crystal **A** crystallized as a monoclinic system, where one $\mathbf{I}_1$–3CNQ-F_4 molecule with a Type I conformation ($\theta_3 = 43.2°$) was crystallographically independent (Figure 1a). The indoline and 3CNQ parts were nearly orthogonal to each other ($\theta_2 + \theta_3 = 78.9°$). This angle is the largest among the Type I $\mathbf{I}_n$–3CNQ-R molecules in the present study, and reflects the single bond nature of bonds ***b*** and ***d*** and the large δ value of this molecule (vide infra). Both indoline and 3CNQ moieties individually formed face-to-face dimers having inversion centers and interplanar distances of 3.38 and 3.36 Å, respectively (red and yellow areas in Figures 1b–1d). These dimers were arranged alternately along the [101] direction to form a one-dimensional structure (Figures 1c and 1d). In addition, a stack between indoline and 3CNQ moieties with ≈3.5 Å interplanar distance was observed (green arrows in Figure 1b), forming a one-dimensional column along the [110] and [1$\bar{1}$0] directions.

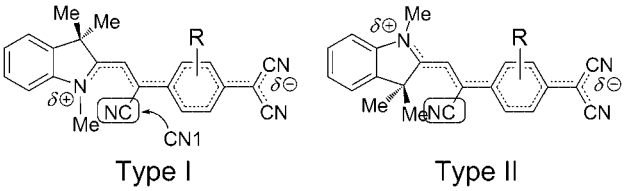

Scheme 3. Two conformational isomers of $\mathbf{I}_1$–3CNQ-R (Type I and II).

Table 1. Conformation and Twist Angles (θ_1–θ_3) of $\mathbf{I}_n$–3CNQ-R Molecules in the Crystal Structures

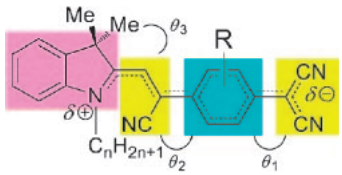

Compound		Type	θ_1/°	θ_2/°	θ_3/°
$\mathbf{I}_1$–3CNQ-F_4	**A**	I	1.4	35.8	43.2
$\mathbf{I}_6$–3CNQ-CF_3	**B**	II	2.0	4.3	162.5
$\mathbf{I}_1$–3CNQ-F_2	**C**	I	9.9	20.3	50.4
$\mathbf{I}_1$–3CNQ-F_1a	**Da**$^{\mathbf{I}}$	II	12.0	4.5	165.0
	Da$^{\mathbf{II}}$	II	7.9	15.8	177.8
$\mathbf{I}_1$–3CNQ-F_1b	**Db**	I	11.1	19.3	48.8
	Dc	I	3.8	17.9	57.3
$\mathbf{I}_1$–3CNQ-$(MeO)_2$	**Ea**	I	1.9	11.8	47.2
	Eb	I	1.5	7.4	—[a)]
$\mathbf{I}_1$–3CNQ-$(EtO)_2$	**Fa**	I	1.4	11.1	48.2
	Fb	I	0.6	5.5	39.7

a) Due to the rotational disorder of the indoline moiety, θ_3 was not obtained for **Eb**.

$\mathbf{I}_6$–3CNQ-CF_3 (B): $\mathbf{I}_6$–3CNQ-CF_3 crystallized as a triclinic system, and one $\mathbf{I}_6$–3CNQ-CF_3 molecule with a Type II conformation ($\theta_3 = 162.5°$) was crystallographically independent (Figures 2a and 2b). In this crystal, only one positional isomer was observed, in which the CF_3 group was connected at the 6-position of the 3CNQ moiety (Chart 1). The small θ_1 and θ_2 angles (2.0 and 4.3°, respectively) reflect the planar molecular structure (Figure 2b). In the crystal structure, the 3CNQ moiety formed a face-to-face dimer in a head-to-tail manner with an interplanar distance of 3.57 Å (yellow areas in Figure 2c). In addition, the dimers stacked at the indoline and 3CNQ moieties with an interplanar distance of ≈3.8 Å (green arrows in Figure 2c) to form a one-dimensional column along the *b* axis. Significant interaction between the indoline moieties was not observed in this crystal. The hexyl group, which extended perpendicularly to the molecular plane (Figure 2a), aggregated to form a one-dimensional structure parallel to the D–π–A column (*b* axis, blue areas in Figures 2c and 2d). Such self-assembling nature involving the cooperation of face-to-face stacks of the D–π–A skeleton and aggregation of alkyl chains resembles those in $\mathbf{I}_n$–3CNQ-H[43] and other D–3CNQ-R derivatives[6,50] having long *N*-alkyl chains.

($\mathbf{I}_1$–3CNQ-F_2)$(MeCN)_{0.5}$ (C) and ($\mathbf{I}_1$–3CNQ-F_1b)-$(MeCN)_{0.5}$ (Db): Crystals **C** and **Db** were iso-structures. In crystal **C**, the $\mathbf{I}_1$–3CNQ-F_2 molecule had a Type I conformation ($\theta_3 = 50.4°$, Figure 3a). Fluorine atoms located at the 3-

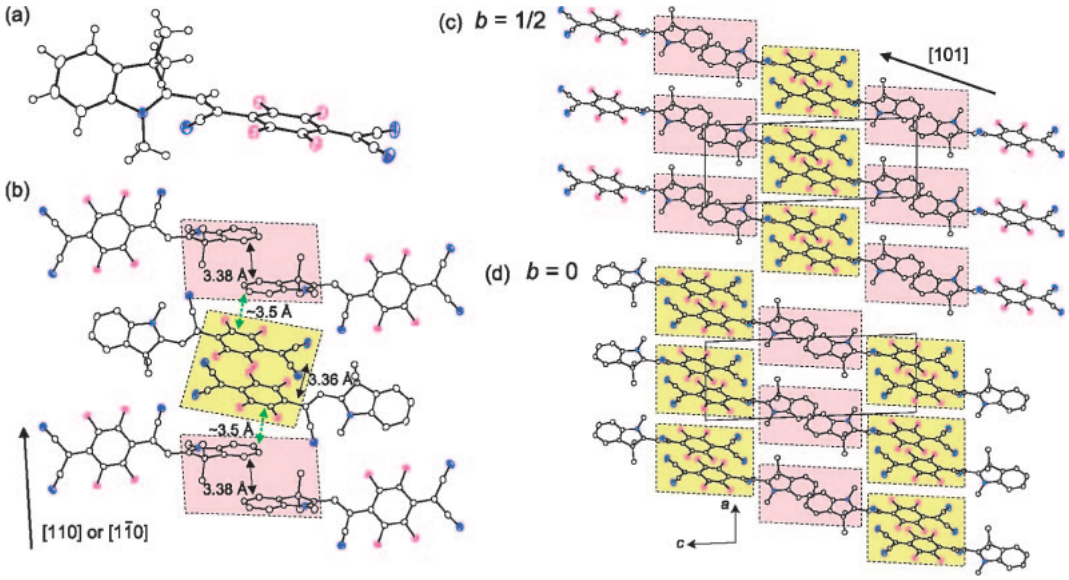

Figure 1. (a) Molecular structure of $\mathbf{I}_1$–3CNQ-F_4 in **A**. (b) One-dimensional column of $\mathbf{I}_1$–3CNQ-F_4 molecules composed of the 3CNQ–3CNQ (yellow area), indoline–indoline (red areas), and indoline–3CNQ (green arrows) stacks. (c) and (d) Molecular packing viewed along the b axis at $b = 1/2$ and 0, respectively. Yellow and red areas represent the dimer units of 3CNQ and indoline moieties, respectively. Hydrogen atoms are omitted in (b)–(d).

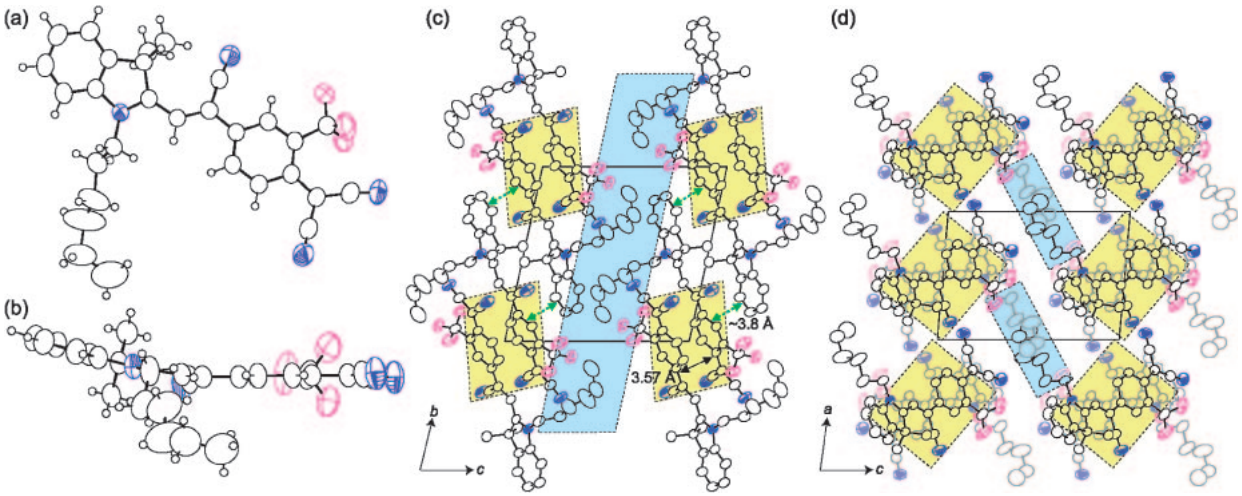

Figure 2. (a) Top view and (b) side view of the molecular structure of $\mathbf{I}_6$–3CNQ-CF_3 in **B**. (c) and (d) Molecular packing of **B** viewed along the a and b axis, respectively, showing a one-dimensional D–π–A column and alkyl chain aggregation. Yellow and blue areas represent the 3CNQ dimers and alkyl chain aggregations, respectively, and green arrows show indoline–3CNQ stacks. Hydrogen atoms are omitted in (c) and (d).

and 6-positions of the 3CNQ moiety, and positional and rotational disorders were not observed. The short C–H···F intramolecular hydrogen bond (2.21 Å) stabilized the 3,6-F_2 isomer rather than the 2,5-F_2 isomer. In addition, steric repulsion between CN1 group and fluorine atom (Scheme 3), which is expected for the 2,5-F_2 isomer, is not present in the 3,6-F_2 isomer. In the crystal structure of **C**, the 3CNQ moiety formed a face-to-face dimer having an inversion center with an interplanar distance of 3.41 Å (yellow areas in Figures 3c and 3d). The dimers interacted with the indoline–3CNQ stacks at a face-to-face distance of ≈3.3 Å to form a one-dimensional column (green arrows in Figure 3d). MeCN solvent molecules were located between 3CNQ dimers (Figure 3d).

$\mathbf{I}_1$–3CNQ-F_1b in **Db** had a Type I conformation (Figure 3b), and the planarity of the D–π–A skeleton expressed by the dihedral angles θ_1–θ_3 was very close to that of **C** (Table 1). This crystal contained only 3-F isomer and showed a short C–H···F intramolecular hydrogen bond (2.19 Å). Further, the molecular packing was very similar to that of **C**, where the face-to-face distance within 3CNQ dimer was 3.39 Å.

$\mathbf{I}_1$–3CNQ-$\mathbf{F}_1$a (Da): Crystal **Da** crystallized as a triclinic system, and two crystallographically independent molecules ($\mathbf{Da}^{\mathbf{I}}$ and $\mathbf{Da}^{\mathbf{II}}$) were observed. $\mathbf{Da}^{\mathbf{I}}$ molecule included two rotational isomers, where 2-F and 6-F isomers exist in a 0.85:0.15 ratio (Figure 4a). On the other hand, $\mathbf{Da}^{\mathbf{II}}$ molecule consisted of 2-F and 3-F positional isomers in a 0.83:0.17 ratio

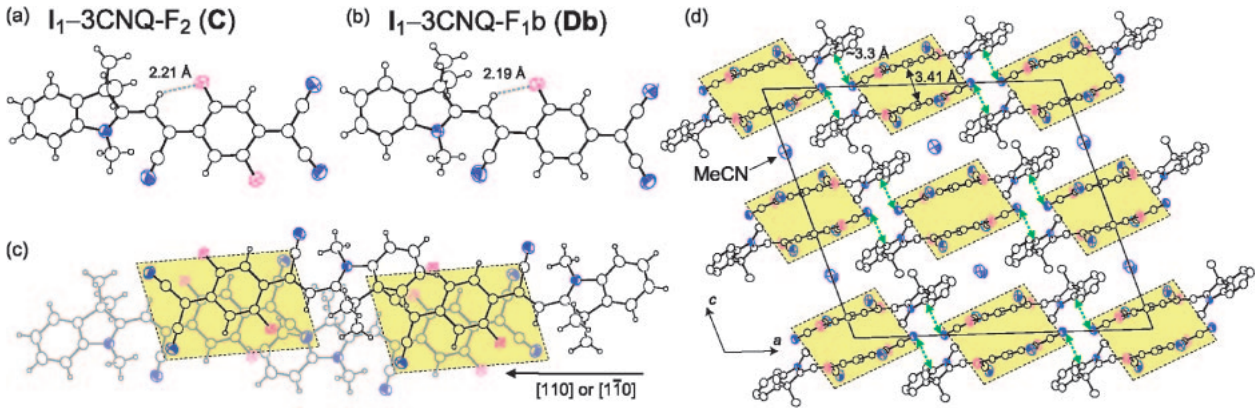

Figure 3. Molecular structures of (a) $\mathbf{I}_1$–3CNQ-F_2 in **C** and (b) $\mathbf{I}_1$–3CNQ-F_1b in **Db**. (c) Overlap mode of a one-dimensional structure in **C**. (d) Molecular packing of **C** viewed along the *b* axis. Yellow areas indicate 3CNQ dimers, and green arrows show indoline–3CNQ stacks. Hydrogen atoms are omitted in (d).

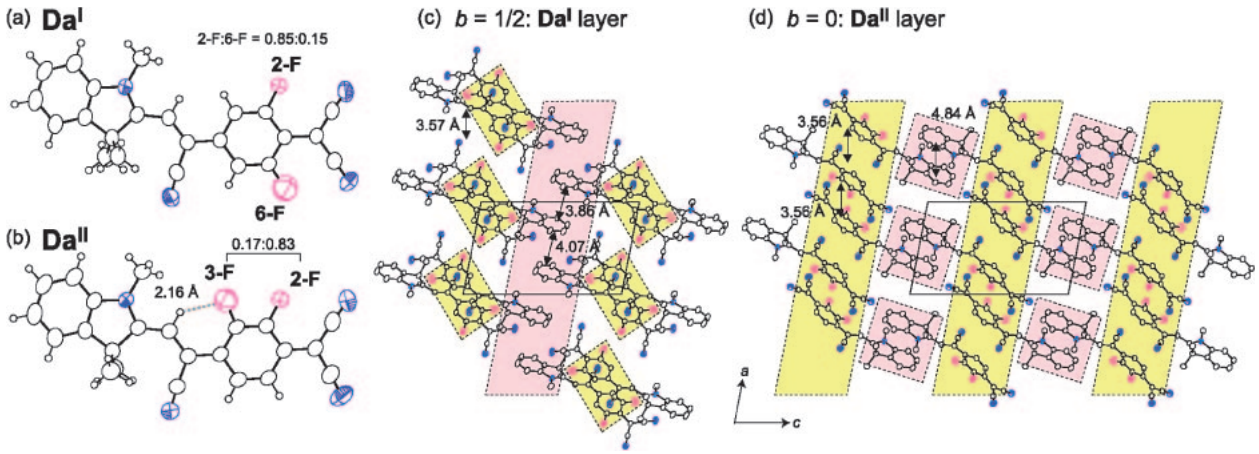

Figure 4. (a) and (b) Molecular structures of $\mathbf{I}_1$–3CNQ-F_1a, $\mathbf{Da}^{\mathbf{I}}$ and $\mathbf{Da}^{\mathbf{II}}$, respectively. (c) and (d) Molecular packing of **Da** viewed along the *b* axis at $b = 1/2$ ($\mathbf{Da}^{\mathbf{I}}$ layer) and $b = 0$ ($\mathbf{Da}^{\mathbf{II}}$ layer), respectively. Red and yellow areas indicate indoline–indoline and 3CNQ–3CNQ stacks, respectively. Hydrogen atoms are omitted in (c) and (d).

(Figure 4b). The distance between a hydrogen atom of the cyanoethene group and a fluorine atom in the 3-F isomer was 2.16 Å (Figure 4b). In this crystal, both $\mathbf{Da}^{\mathbf{I}}$ and $\mathbf{Da}^{\mathbf{II}}$ molecules had a Type II conformation (Figures 4a and 4b), and their molecular structures were more planar than that of the **Db** and **Dc** molecules having a Type I conformation (Table 1). $\mathbf{Da}^{\mathbf{I}}$ and $\mathbf{Da}^{\mathbf{II}}$ molecules individually formed layer structures on the $b = n + 1/2$ and $n + 0$ planes, respectively. In the $\mathbf{Da}^{\mathbf{I}}$ layer, the 3CNQ moiety formed an isolated face-to-face dimer with an interplanar distance of 3.57 Å (yellow areas), whereas the indoline moiety formed a segregated column along the *a* axis with non-uniform interplanar distances of 3.86 and 4.07 Å (red areas in Figure 4c). In the $\mathbf{Da}^{\mathbf{II}}$ layer, the 3CNQ moiety formed a segregated column along the *a* axis with interplanar distances of 3.56 Å (yellow areas), whereas the indoline moiety formed an isolated dimer with a face-to-face distance of 4.84 Å (Figure 4d).

$\mathbf{I}_1$–3CNQ-$\mathbf{F}_1$b (Dc): Crystal **Dc** crystallized as a monoclinic system, where the $\mathbf{I}_1$–3CNQ-F_1b molecule with a Type I conformation is crystallographically independent ($\theta_3 = 57.3°$, Figure 5a). A fluorine atom was located at the 3-position of the 3CNQ moiety, and a short C–H···F intramolecular hydrogen bond (2.19 Å) was observed. In the crystal structure of **Dc**, the 3CNQ moiety formed a face-to-face dimer with an interplanar distance of 3.33 Å and an inversion center (yellow areas in Figures 5b and 5c). The 3CNQ dimers were connected by the indoline–indoline stacks to form a one-dimensional structure along the *b* axis (Figure 5b). The indoline moiety formed a segregated column along the *a* axis with non-uniform interplanar distances of 3.39 and 3.64 Å (Figure 5c).

$\mathbf{I}_1$–3CNQ-$(\mathbf{MeO})_2$ (Ea and Eb): Two polymorphs of $\mathbf{I}_1$–3CNQ-$(MeO)_2$ (**Ea** and **Eb**) were obtained from the same batch. In the crystal **Ea**, the $\mathbf{I}_1$–3CNQ-$(MeO)_2$ molecule had a Type I conformation ($\theta_3 = 47.2°$) and contained two rotational isomers, where 2,5- and 3,6-isomers existed in a 0.40:0.60 ratio (Figure 6a). The terminal dicyanomethylene group was nearly parallel to the benzenoid plane ($\theta_1 = 1.9°$). The 3CNQ and indoline moieties individually stacked to form one-dimensional columns along the *b* axis and [110] direction, respectively (yellow and red areas in Figures 6b and 6c). Each face-to-face stack had a head-to-tail orientation to cancel the dipole moment. The interplanar distances were 3.51 and 3.68 Å for the 3CNQ column and 3.48 and 3.85 Å for the indoline column.

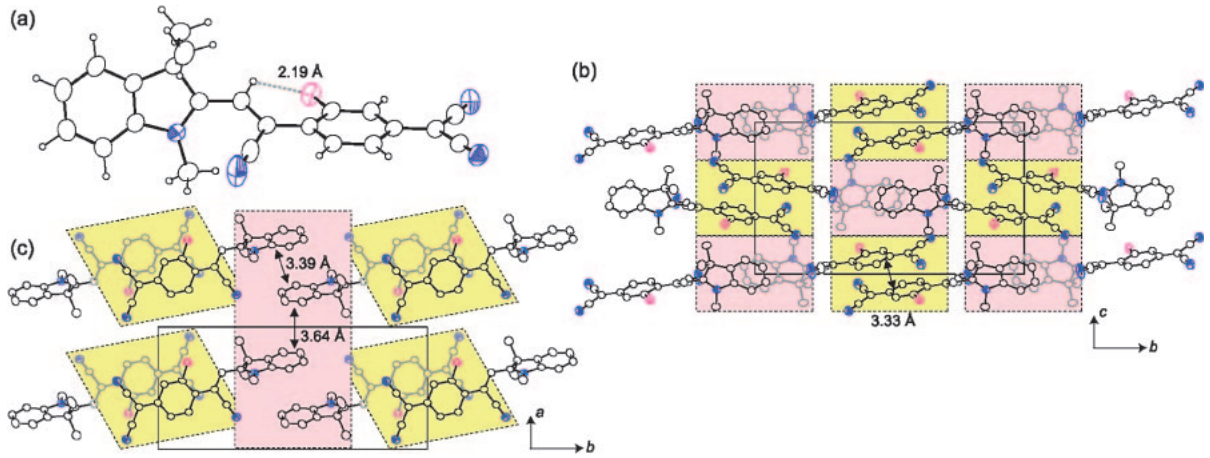

Figure 5. (a) Molecular structure of $\mathbf{I}_1$–3CNQ-F_1b in **Dc**. (b) and (c) Molecular packing of **Da** viewed along the *a* and *c* axis, respectively. Red and yellow areas indicate indoline–indoline and 3CNQ–3CNQ stacks, respectively. Hydrogen atoms are omitted in (b) and (c).

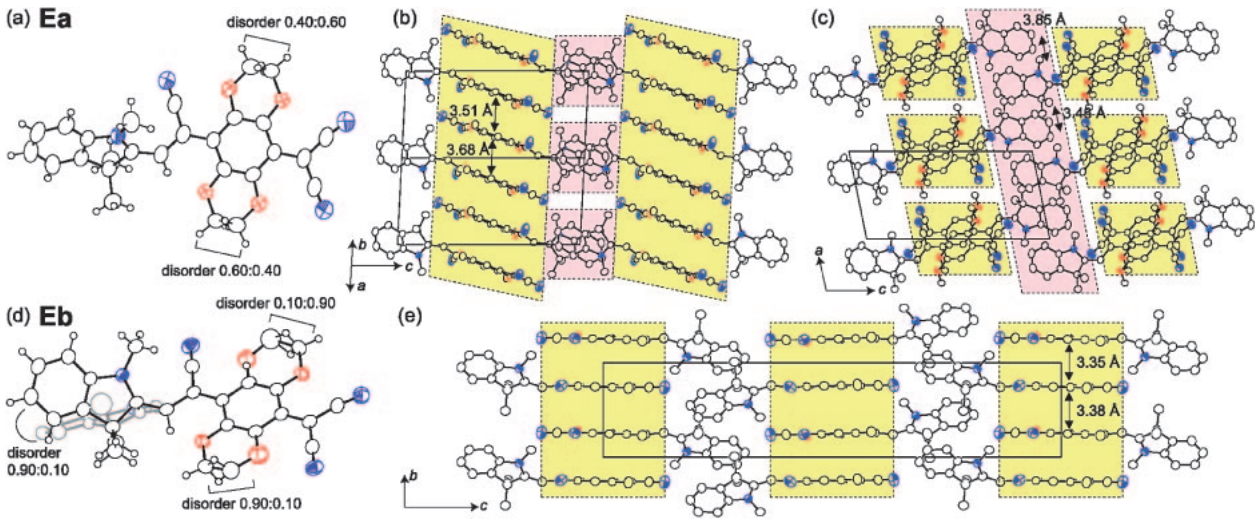

Figure 6. (a) Molecular structure of the $\mathbf{I}_1$–3CNQ-$(MeO)_2$ in **Ea**. (b) and (c) Molecular packing of **Ea** viewed along the [110] direction and *b* axis, respectively. (d) Molecular structure of the $\mathbf{I}_1$–3CNQ-$(MeO)_2$ in **Eb**. The gray atoms are those of the disordered indoline moiety. (e) Molecular packing of **Eb** viewed along the *a* axis. Yellow and red areas show the 3CNQ–3CNQ and indoline–indoline stacks, respectively. Hydrogen atoms are omitted in (b), (c), and (e). The disordered atoms of smaller site occupancy factors are also omitted for clarity in (b), (c), and (e).

Similar to **Ea**, the $\mathbf{I}_1$–3CNQ-$(MeO)_2$ molecule in **Eb** had a Type I conformation. A rotational disorder of the indoline moiety (0.90:0.10 ratio) was observed, where dihedral angles (θ_3) were ≈41 and 45°, respectively (Figure 6d). A rotational disorder of the 3CNQ moiety was also observed, where 3,6- and 2,5-isomers existed in a 0.90:0.10 ratio (Figure 6d). The terminal dicyanomethylene group was nearly parallel to the benzenoid plane ($\theta_1 = 1.5°$). In the crystal structure, the 3CNQ moiety stacked in a head-to-tail fashion with interplanar distances of 3.35 and 3.38 Å to form a one-dimensional column along the *b* axis (yellow areas in Figure 6e). In contrast to **Ea**, the indoline moiety did not form π-stacking structures and was arranged in a herringbone motif in the *ab* plane (Figure 6e).

($\mathbf{I}_1$–3CNQ-$(EtO)_2$)(MeCN) (Fa) and $\mathbf{I}_1$–3CNQ-$(EtO)_2$ (Fb): Two polymorphs of $\mathbf{I}_1$–3CNQ-$(EtO)_2$ (**Fa** and **Fb**) were obtained from the same batch. In the solvated crystal **Fa**, the $\mathbf{I}_1$–3CNQ-$(EtO)_2$ molecule had a Type I conformation ($\theta_3 = 48.2°$, Figure 7a). Rotational disorder of the 3CNQ moiety was not observed. The terminal dicyanomethylene group was nearly parallel to the benzenoid plane ($\theta_1 = 1.4°$), whereas the π-bridge was distorted towards the benzenoid plane ($\theta_2 = 11.1°$). The 3CNQ and indoline moieties stacked individually to form one-dimensional columns along the *a* axis and [110] direction, respectively (yellow and red areas in Figures 7b and 7c). Each face-to-face stack had a head-to-tail orientation to cancel the dipole moment. The interplanar distances were 3.43 and 3.52 Å for the 3CNQ column and 3.41 and 5.03 Å for the indoline column. These structural features are similar to those of **Ea** (Figures 6b and 6c).

Similar to **Fa**, the $\mathbf{I}_1$–3CNQ-$(EtO)_2$ molecule in the non-solvated crystal **Fb** had a Type I conformation with a dihedral angle $\theta_3 = 39.7°$ (Figure 7d). Rotational disorder of the 3CNQ

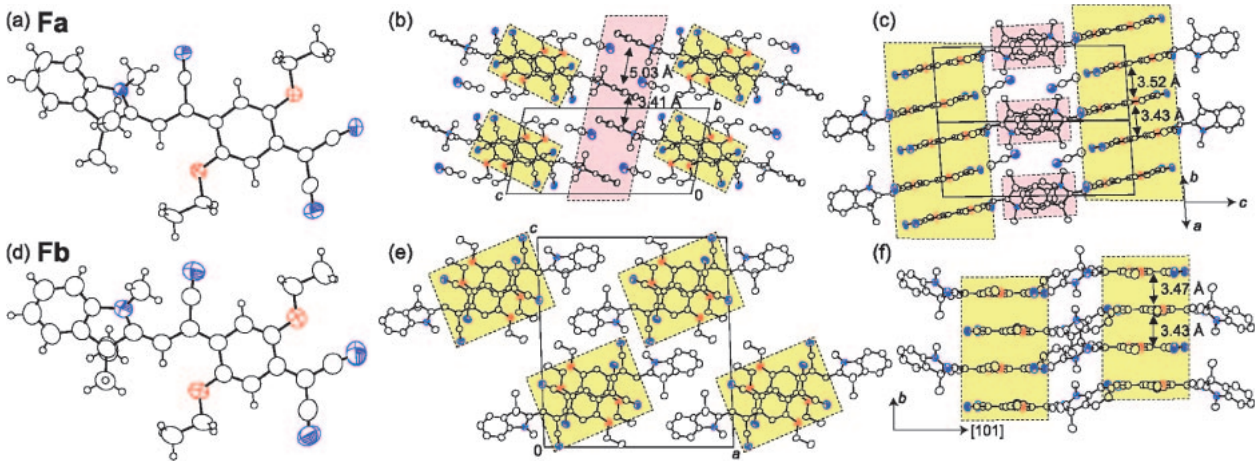

Figure 7. (a) Molecular structure of the $\mathbf{I}_1$–3CNQ-$(EtO)_2$ in **Fa**. (b) and (c) Molecular packing of **Fa** viewed along the *a* axis and [110] direction, respectively. (d) Molecular structure of $\mathbf{I}_1$–3CNQ-$(EtO)_2$ in **Fb**. (e) and (f) Molecular packing of **Fb** viewed along the *b* axis and the molecular short axis, respectively. Red and yellow areas show the indoline–indoline and 3CNQ–3CNQ stacks, respectively. Hydrogen atoms are omitted in (b), (c), (e), and (f).

Table 2. Selected Intramolecular Bond Lengths (***a*–*e***, Å) and Bond Length Ratio (*BLR*) of $\mathbf{I}_n$–3CNQ-R Molecules in the Crystal Structures

Compound		Type	***a***/Å	***b***/Å	***c***/Å	***d***/Å	***e***/Å	*BLR*
$\mathbf{I}_1$–3CNQ-F_4	**A**	I	1.313(2)	1.440(3)	1.350(3)	1.457(3)	1.427(3)	1.624(3)
$\mathbf{I}_6$–3CNQ-CF_3	**B**	II	1.348(3)	1.412(4)	1.384(4)	1.439(4)	1.426(4)	1.566(4)
$\mathbf{I}_1$–3CNQ-F_2	**C**	I	1.312(2)	1.435(3)	1.356(3)	1.451(3)	1.423(3)	1.615(3)
$\mathbf{I}_1$–3CNQ-F_1a	$\mathbf{Da}^{\mathbf{I}}$	II	1.341(3)	1.415(3)	1.372(3)	1.453(3)	1.427(3)	1.583(3)
	$\mathbf{Da}^{\mathbf{II}}$	II	1.348(3)	1.404(3)	1.387(3)	1.441(4)	1.410(4)	1.556(4)
$\mathbf{I}_1$–3CNQ-F_1b	**Db**	I	1.320(3)	1.428(3)	1.366(3)	1.449(3)	1.419(3)	1.599(3)
	Dc	I	1.315(4)	1.436(5)	1.358(5)	1.451(5)	1.418(5)	1.611(5)
$\mathbf{I}_1$–3CNQ-$(MeO)_2$	**Ea**	I	1.349(2)	1.386(2)	1.400(2)	1.416(2)	1.404(2)	1.530(2)
	Eb	I	—[a]	1.375(6)	1.422(5)	1.416(5)	1.400(5)	—[a]
$\mathbf{I}_1$–3CNQ-$(EtO)_2$	**Fa**	I	1.357(6)	1.379(7)	1.391(7)	1.420(7)	1.407(7)	1.531(8)
	Fb	I	1.348(6)	1.389(7)	1.411(7)	1.423(7)	1.399(7)	1.526(7)

a) Not obtained due to the rotational disorder of the indoline moiety.

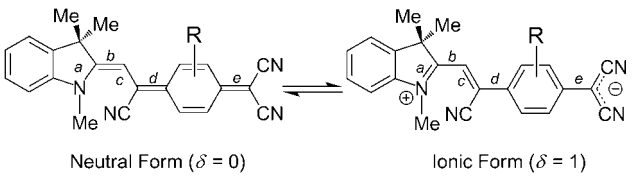

Scheme 4. Bond alternations of $\mathbf{I}_1$–3CNQ-R in neutral ($\delta = 0$) and ionic ($\delta = 1$) forms.

moiety was not observed. The 3CNQ moiety had a planar structure ($\theta_1 = 0.6°$ and $\theta_2 = 5.5°$). In the crystal structure, the 3CNQ moiety stacked in a head-to-tail manner with interplanar distances of 3.43 and 3.47 Å to form a one-dimensional column along the *b* axis (yellow areas in Figures 7e and 7f). In contrast to **Fa**, the indoline moiety did not form π-stacking structures.

Structural Parameters Related to Molecular and Electronic Structures of $\mathbf{I}_n$–3CNQ-R. (A) Bond Length Ratio (*BLR*) vs. Degree of Intramolecular CT: Electronic structure of an $\mathbf{I}_n$–3CNQ-R molecule is presented by the mixing of two resonance structures of neutral ($\delta = 0$) and ionic ($\delta = 1$) forms (Scheme 4). In a previous report, we proposed a methodology to qualitatively estimate the degree of intramolecular CT (δ) of $\mathbf{I}_n$–3CNQ-R using the bond alternation in these two forms.[43] The bond length ratio defined as ($BLR = (\boldsymbol{b} + \boldsymbol{d} + \boldsymbol{e})/(\boldsymbol{a} + \boldsymbol{c})$) is the best experimental parameter to discuss the δ value in the solid state, and shows a good linear relationship with the dipole moments and δ values estimated from MO calculation.[43] It should be noted that we can not quantitatively discuss δ values from *BLR* analysis, since the $\delta = 0$ and 1 limits for the $\mathbf{I}_n$–3CNQ-R system have not been obtained at present. The *BLR* values obtained for $\mathbf{I}_1$–3CNQ-R derivatives and $\mathbf{I}_6$–3CNQ-CF_3 are summarized in Table 2 together with the bond lengths ***a*–*e***. It is noteworthy that the *BLR* value well reflects the δ value; for Type I derivatives, it decreases in the order R = F_4, F_2, F_1b, $(MeO)_2$, and $(EtO)_2$, which is in good agreement with the weakening of acceptor strength of the 3CNQ moiety.

(B) Molecular Conformations and Planarity: In the crystal structures, $\mathbf{I}_1$–3CNQ-R molecules except for **Db**, had a Type I conformation. The molecular conformation of $\mathbf{I}_n$–3CNQ-R is determined mainly by the steric repulsion between the CN1 group and the *N*-alkyl group or the 3,3-dimethyl group in the indoline moiety (Scheme 3). Type I conformation

Table 3. Dipole Moments (μ_g and μ_e), Degree of CT (δ_{dipole}), Polarizability (α), and Hyperpolarizabilities (β and γ) of $\mathbf{I}_n$–3CNQ-R Molecules Evaluated by MO Calculation (INDO/S)

Compound		Type	μ_g/D	μ_e/D	δ_{dipole}	$\alpha/10^{-24}$ cm^3	$\beta/10^{-30}$ cm^5 esu^{-1}	$\gamma/10^{-36}$ cm^6 erg^{-1}
$\mathbf{I}_1$–3CNQ-F_4	**A**	I	27.29	10.20	0.73	67.67	−476.9	57.66
$\mathbf{I}_6$–3CNQ-CF_3	**B**	II	20.04	17.87	0.53	69.81	−105.1	−264.5
$\mathbf{I}_1$–3CNQ-F_2	**C**	I	25.93	10.79	0.71	67.51	−408.3	−38.82
$\mathbf{I}_1$–3CNQ-F_1a	**Da**[I a)]	II	19.51	16.50	0.54	74.46	−139.1	−320.5
	Da[II a)]	II	16.75	15.68	0.52	69.24	−75.3	−270.0
$\mathbf{I}_1$–3CNQ-F_1b	**Db**	I	23.77	10.51	0.69	67.80	−363.1	−96.57
	Dc	I	25.46	8.40	0.75	64.68	−432.6	39.13
$\mathbf{I}_3$–3CNQ-H	**3a**[b)]	I	22.59	13.14	0.63	71.01	−298.5	−206.1
$\mathbf{I}_{10}$–3CNQ-H	**10**[b)]	I	21.87	12.71	0.63	70.12	−291.0	−203.2
$\mathbf{I}_1$–3CNQ-$(MeO)_2$	**Ea**[a)]	I	15.88	15.71	0.50	64.66	−55.9	−227.3
$\mathbf{I}_1$–3CNQ-$(EtO)_2$	**Fa**	I	17.07	15.18	0.53	67.14	−94.6	−249.3
	Fb	I	15.54	16.04	0.49	64.46	−37.2	−221.4

a) Orientation disorders of substituent groups on the 3CNQ moieties were observed. MO calculations were performed using structures having larger occupancies. b) See, reference 43.

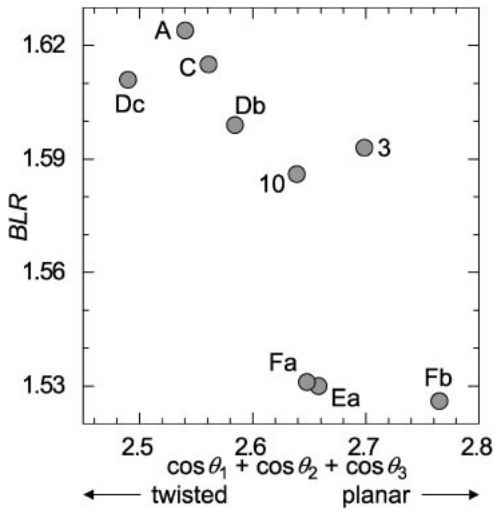

Figure 8. Plot of *BLR* value vs. molecular planarity ($\cos\theta_1 + \cos\theta_2 + \cos\theta_3$) for Type I $\mathbf{I}_1$–3CNQ-R molecules together with $\mathbf{I}_3$–3CNQ-H (**3**; *BLR* = 1.593(2), molecular planarity = 2.70) and $\mathbf{I}_{10}$–3CNQ-H (**10**; 1.586(2), 2.64) (R = H).[43]

of $\mathbf{I}_1$–3CNQ-R molecules is caused by the smaller size of the *N*-methyl group than that of the 3,3-dimethyl group. This is in contrast to what is observed for most of the long alkyl chain $\mathbf{I}_n$–3CNQ derivatives[43] and $\mathbf{I}_6$–3CNQ-CF_3 (**B**) having a Type II conformation. In a previous study, we also clarified that the Type I molecule has a larger δ value than that of Type II.[43] The considerably smaller *BLR* value of Type II molecule **B** (R = CF_3, 1.566(4)), which should be similar to that of Type I molecule **C** (R = F_2, 1.615(3)) according to the acceptor strength, is also in good agreement with the above tendency.

The δ value of a $D^{\delta+}$–π–$A^{\delta-}$ compound is expected to relate to its molecular planarity. In the ionic form ($\delta = 1$, Scheme 4), bonds ***b***, ***d***, and ***e*** have a single bond character and can twist to have large dihedral angles θ_1, θ_2, and θ_3, respectively. On the other hand, the neutral form ($\delta = 0$) has a planar structure because of the double bond character of these bonds. Such expectation has been theoretically demonstrated in some $D^{\delta+}$–π–$A^{\delta-}$ compounds.[41,51] Figure 8 plots the *BLR* value against molecular planarity defined as $\cos\theta_1 + \cos\theta_2 + \cos\theta_3$ for Type I $\mathbf{I}_1$–3CNQ-R molecules and Type I $\mathbf{I}_n$–3CNQ-H (n = 3 and 10).[43] As expected, the *BLR* value increases with the decrease in molecular planarity, indicating that a twisted D–π–A skeleton results in a highly ionic form. For the Type II molecules, we could not find such a relationship between *BLR* and molecular planarity because of the small difference in planarity.

(C) Dipole Moments and Degree of Intramolecular CT: The δ value of a $D^{\delta+}$–π–$A^{\delta-}$ molecule is related to molecular properties such as dipole moments (ground state, $\mu_g = \delta ed$; excited state, $\mu_e = (1 - \delta)ed$, where e and d are the elementary electric charge and the average distance between centers of positive and negative charges, respectively). In the previous paper, we demonstrated that the μ_g values of $\mathbf{I}_n$–3CNQ-R molecules obtained by a MO calculation based on the crystal structures show a good relationship with the *BLR* values.[43] The degree of CT (δ_{dipole}) reproducing dipole moments is evaluated using eq 4.

$$\delta_{dipole} = \frac{\mu_g}{\mu_e + \mu_g} \tag{4}$$

Table 3 lists the calculated μ_g, μ_e, and δ_{dipole} values. The δ_{dipole} value for Type I derivatives increases in the order R = $(EtO)_2$ and $(MeO)_2$, F_1b, F_2, and F_4, which is in good agreement with strengthening of the acceptor strength of 3CNQ moiety. Similar to the tendency found in the *BLR* analysis, the δ_{dipole} values for Type II molecules are smaller than those for Type I molecules. The δ_{dipole} value reflects the molecular shape, conformation, and substitution effects on the spatial charge distribution, and is regarded as an appropriate parameter to express the δ values.

Molecular (Hyper)polarizabilities and Degree of Intramolecular CT. Equation 5 represents the relationship of molecular polarization (p) under an electric field (E) with molecular polarizability (α) and hyperpolarizabilities (β and γ).

$$p = \mu_g + \alpha E + \beta E^2 + \gamma E^3 + \ldots \tag{5}$$

Polarizabilities α and β are approximated by the two-level model,

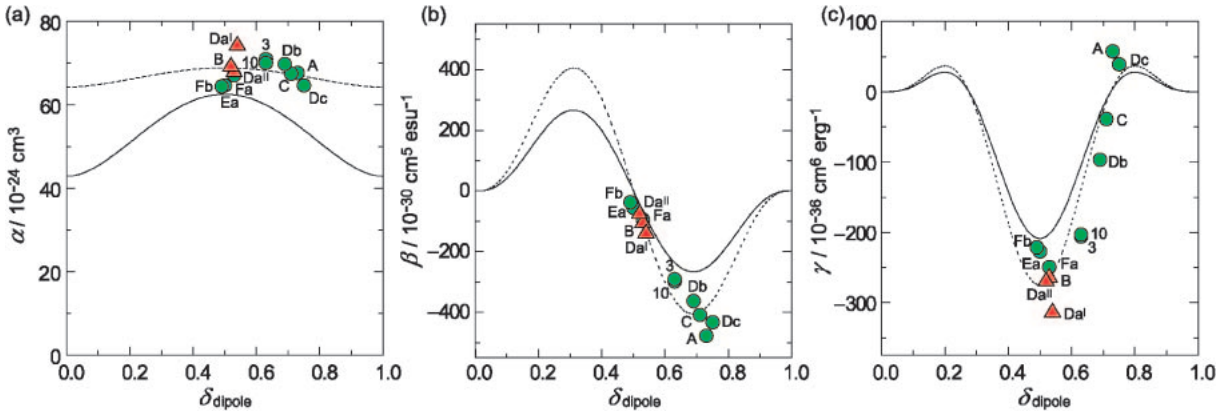

Figure 9. Plots of (hyper)polarizabilities α (a), β (b), and γ (c) obtained by the MO calculation against δ_{dipole} for $\mathbf{I}_1$–3CNQ-R, $\mathbf{I}_6$–3CNQ-CF_3, and $\mathbf{I}_n$–3CNQ-H (**3**: $n = 3$ and **10**: $n = 10$)[43] molecules. Green circles and red triangles show Type I and II molecules, respectively. Solid lines are the theoretical curves calculated from eqs 10–12; $\alpha = 3.15 \times 10^2\delta^2(1-\delta)^2 + 42.9$, $\beta = 7.17 \times 10^4\delta^3(1-\delta)^3(1-2\delta)$, and $\gamma = 2.14 \times 10^5\delta^4(1-\delta)^4(1-5\delta+5\delta^2)$. Dashed lines are the least-squares fittings for each plot; $\alpha = 7.32 \times 10^1\delta^2(1-\delta)^2 + 64.3$, $\beta = 1.09 \times 10^5\delta^3(1-\delta)^3(1-2\delta)$, and $\gamma = 2.82 \times 10^5\delta^4(1-\delta)^4(1-5\delta+5\delta^2)$.

$$\alpha \propto {\mu_{eg}}^2/E_{eg} \tag{6}$$

$$\beta \propto {\mu_{eg}}^2(\mu_e - \mu_g)/{E_{eg}}^2 \tag{7}$$

Here, E_{eg} is the energy difference between ground and excited states, and μ_{eg} is the transition dipole moment which is expressed by eq 8 according to Mulliken's CT theory.[52]

$$\mu_{eg} = \delta^{1/2}(1-\delta)^{1/2}ed \tag{8}$$

γ is approximated by the three-level model,[15]

$$\gamma \propto [{\mu_{eg}}^2(\mu_e - \mu_g)^2 - {\mu_{eg}}^4]/{E_{eg}}^3 + {\mu_{eg}}^2{\mu_{e'e}}^2/{E_{eg}}^2E_{e'g} \tag{9}$$

where e′ is the second excited state.

It is essential to have a large d value for the improvement in the α, β, and γ values. The δ value is also important according to the theoretical treatment by Ducuing and Flytzanis based on the point charge model.[53] The α and β values can be approximated using the δ value in eqs 10 and 11, respectively.

$$\alpha \propto \delta^2(1-\delta)^2 \tag{10}$$

$$\beta \propto \delta^3(1-\delta)^3(1-2\delta) \tag{11}$$

The γ value cannot be expressed explicitly by the δ value without the $\mu_{e'e}$ and $E_{e'g}$ values (eq 9). Since the two-level model is applicable for the non-centrosymmetric $\mathbf{I}_n$–3CNQ-R derivatives, the second term in eq 9 is negligible, leading to eq 12.

$$\gamma \propto [{\mu_{eg}}^2(\mu_e - \mu_g)^2 - {\mu_{eg}}^4]/{E_{eg}}^3 \propto \delta^4(1-\delta)^4(1-5\delta+5\delta^2) \tag{12}$$

Equations 10–12 indicate that (1) the α value has a maximum at $\delta = 0.5$ and minima at $\delta = 0$ and 1; (2) the $|\beta|$ value has maxima at $\delta = 0.31$ and 0.69 and minima at $\delta = 0$, 0.5, and 1; and (3) the $|\gamma|$ value has maxima at $\delta = 0.2$, 0.5, and 0.8 and minima at $\delta = 0$, 0.28, 0.72, and 1 (Figure 9). These relationships of α, β, and γ values with δ are similar to those obtained against bond length alternation (*BLA*) demonstrated by Marder et al.[15] or mixing between the limiting-resonance forms by Barzoukas et al.[16]

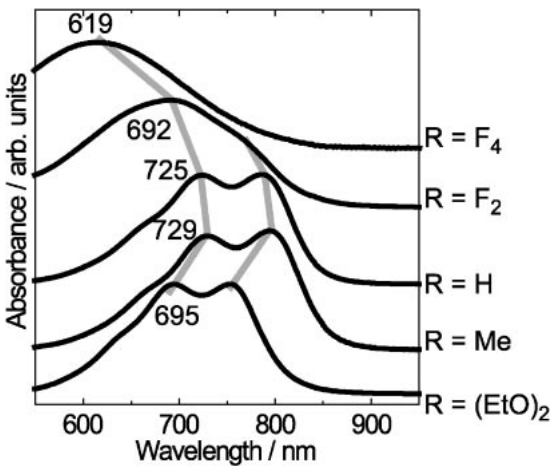

Figure 10. Intramolecular CT absorption in UV–vis spectra of $\mathbf{I}_1$–3CNQ-R derivatives (R = F_4, F_2, H, Me, and $(EtO)_2$) in MeCN solution.

Figure 9 plots (hyper)polarizabilities (α, β, and γ) obtained by the MO calculation against δ_{dipole} value together with the modified theoretical curves based on eqs 10–12. Relatively good correlations between calculated values and theoretical curves confirm that δ is a fundamental parameter to describe (hyper)polarizabilities. The most important consequence is that these non-linear optical parameters of $D^{\delta+}$–π–$A^{\delta-}$ molecule have maximum absolute values at partial δ values ($0 < \delta < 1$) and that they can be modulated by chemical modifications of the D- and A-moieties.

Solution State Properties. (A) Absorption Spectra and Degree of Intramolecular CT in Solution: $D^{\delta+}$–π–$A^{\delta-}$ compounds derived from amines and TCNQ derivatives are known to exhibit characteristic broad and intense intramolecular CT absorption bands in the range of 600–900 nm with one or two major peaks in the solution state.[6,7,14,25a] In the $\mathbf{I}_1$–3CNQ-R system, similar spectra were obtained with two major peaks (Figure 10), which are summarized in Table 4.

The energy of an intramolecular CT for the ionic ground state ($\delta > 0.5$) ($h\nu_{CT}^{I}$: Symbol I means the ionic ground state)

Table 4. UV–Vis Spectra and the δ_{solv} Values of $\mathbf{I}_n$–3CNQ-R Derivatives

R (E^A/V)[a]	UV–vis[b]/nm								
	MeOH	MeCN	Acetone	PhCl	Dioxane	PhH	PhMe	CS_2	δ_{solv}
F_4 (+0.60)	—[d], 574	—[d], 619	—[d], 636	802, 731	796, 725	—[c]	—[c]	—[c]	0.77
CF_3 ($n = 1$) (+0.44)	765sh, 661	770sh, 690	776sh, 708	801, 731	789, 724	795sh, 725	800sh, 722	—[c]	0.61
CF_3 ($n = 6$) (+0.44)	756, 716	771, 722	780, 728	814, 743	800, 732	799, 734	797, 732	803, 736	0.54
F_2 (+0.41)	770sh, 657	770sh, 692	775sh, 704	803, 728	791, 718	795, 719	794, 719	801, 727	0.62
F_1a (+0.32)	790, 720	786, 729	793, 730	809, 735	785sh, 716	795sh, 717	790sh, 712	790sh, 719	0.52
F_1b (+0.32)	770sh, 686	765sh, 699	765sh, 705	794, 722	784, 711	785, 714	782, 712	788, 718	0.55
H (+0.22)	779, 720	787, 725	792, 726	794, 726	785sh, 710	780sh, 700	785sh, 701	785sh, 707	0.51
Me (+0.20)	789, 726	795, 729	800, 731	800sh, 723	790sh, 705	780sh, 703	770sh, 696	775sh, 705	0.50
$(MeO)_2$ (+0.05)	749, 694	752, 696	754, 696	773sh, 693	—[d], 672	—[d], 674	—[d], 669	—[d], 682	0.50
$(EtO)_2$ (+0.01)	750, 694	753, 695	754, 694	771sh, 691	—[d], 668	—[d], 670	—[d], 665	—[d], 678	0.50

a) E^A: Reduction potential of R-TCNQ, V vs. SCE in MeCN. b) Peak position. c) Not measured due to too poor solubility. d) Not found due to overlapping with the second band.

is presented in eq 13,[54] where I_p and E_A are the ionization potential of D and the electron affinity of A moieties, respectively, and ε, r, ΔG, and X are the dielectric constant of the solvent, the average distance between D and A moieties, the difference in solvation energies of D^0–π–A^0 and D^{1+}–π–A^{1-} species, and the resonance stabilization energies of D^0–π–A^0 and D^{1+}–π–A^{1-} species, respectively.

$$h\nu_{CT}{}^{I} = -(I_p - E_A) + (2\delta - 1)\left(\frac{1}{\varepsilon}\frac{e^2}{r} - \Delta G\right) + X \qquad (13)$$

Similarly, the energy for the neutral ground state ($h\nu_{CT}{}^{N}$: Symbol N means the neutral ground state) is presented in eq 14, where X' is the resonance stabilization energy.

$$h\nu_{CT}{}^{N} = (I_p - E_A) + (1 - 2\delta)\left(\frac{1}{\varepsilon}\frac{e^2}{r} - \Delta G\right) - X' \qquad (14)$$

The transition energy ($h\nu_{CT}$) is mainly affected by three terms: chemical structure ($I_p - E_A$), solvent effect (ε and ΔG), and degree of CT (δ). Furthermore, eqs 13 and 14 indicate that the CT energy increases with the increase and decrease of solvent polarity in the ionic ($h\nu_{CT}{}^{I}$, $\delta \geq 0.5$) and neutral ($h\nu_{CT}{}^{N}$, $\delta \leq 0.5$) ground states, respectively.

$\mathbf{I}_1$–3CNQ-R derivatives showed two distinct peaks of which relative intensity depends on the acceptor strength of the 3CNQ-R moiety and solvent polarity. Compounds derived from strong or weak R-TCNQ acceptors exhibited two peaks in less-polar and polar solvents, respectively (Figure 11). Since electrochemical measurement revealed that the ($I_P - E_A$) value of a $\mathbf{I}_1$–3CNQ-R compound is a linear function of the δ values,[1b] the appearance of two separate peaks is thought to relate strongly to the interaction between the δ values and solvent dipoles.

The appearance of two separate peaks in some D–π–A compounds has received a lot of interest, and its origin has been interpreted in several ways[55] such as aggregation phenomena,[19,56] conformational isomerism,[41,57] or vibronically resolved features.[40] For $\mathbf{I}_1$–3CNQ-R compounds, aggregation phenomena are not plausible, since Beer's law is valid. Rotation isomers are not adequate since solid-state spectra exhibited multiple absorption peaks.

(B) Substituent Effect: Intramolecular CT bands of a D–3CNQ-R system shift depending on the chemical structure in accordance with the differences of ($I_p - E_A$) and δ. Absorption maxima of $C_{16}H_{33}$-Q–3CNQ-R[25a] (Q = quinolinium) and DEMI–3CNQ-R[14] (DEMI = diethylammonium, Chart 1) in MeCN shift to higher energy regions by 147 and 58 nm, respectively, because of the modification of R substituents from H to F_4. In the present work, $\mathbf{I}_1$–3CNQ-R derivatives also showed a blue shift of the intramolecular CT absorption bands with increasing electron-withdrawing effect of R substituents from R = Me (729 nm, the second lowest energy peak) to R = F_4 (619 nm) in MeCN (Figure 10 and Table 4). For the $\mathbf{I}_1$–3CNQ-R derivatives with strong electron-donating substituents (R = $(MeO)_2$ and $(EtO)_2$), the bands shifted to higher energy region (696–695 nm) probably because they have a neutral ground state in eq 14.

(C) Solvatochromic Shift: It is known that intramolecular CT absorption bands of a $D^{\delta+}$–π–$A^{\delta-}$ exhibit a hypsochromic shift with increase in solvent polarity.[4a,6–8,54,58,59] A similar solvatochromism was also observed in the $\mathbf{I}_1$–3CNQ-R system. $\mathbf{I}_1$–3CNQ-R derivatives with strong electron-withdrawing groups (R = F_4, CF_3, and F_2) showed significant solvatochromic shifts (Table 4). For example, $\mathbf{I}_1$–3CNQ-F_2 exhibited bands at 770 (shoulder peak) and 657 nm in MeOH, and 803 and 728 nm in PhCl, where the hypsochromic shifts were 33 and 71 nm, respectively (Figure 11a). The shifts became less pronounced with weakening electron-accepting ability of the 3CNQ-R part, and R = H, Me, $(MeO)_2$, and $(EtO)_2$ derivatives hardly exhibited a solvatochromic shift (Figure 11b).

Figure 12 plots the transition energy of the second lowest energy peak ($h\nu_{CT}$(2nd)), which is more clearly and intensely observed than the first one, in polar solvents (MeOH, MeCN, acetone, and PhCl) against transition energy of Reichardt's betain dye (E_T)[5b] as an indicator of solvent polarity. The plots showed a good linear relationship ($h\nu_{CT}(2nd) = aE_T + b$), and the slope a decreased with weakening electron-accepting ability of the 3CNQ-R moiety.

In previous studies,[1b,43] we demonstrated a methodology to estimate the degree of intramolecular CT in the solution state (δ_{solv}) using solvatochromic behavior. Considering that the δ value of an $\mathbf{I}_1$–3CNQ-R is subjected strongly to ($I_p - E_A$) in eq 13 and that $h\nu_{CT}$ shows a linear relationship with E_T, the δ_{solv} value for $\delta \geq 0.5$ is obtained as $(a + 1)/2$. It should be noted that the obtained δ_{solv} values bear some ambiguities due to the difference in the solvation energies (ΔG) between Reichardt's betaine dye and $\mathbf{I}_n$–3CNQ-R compounds, although

the difference should be small compared to whole intramolecular CT energy.[43] The δ_{solv} values obtained for $\mathbf{I}_n$–3CNQ-R derivatives are summarized in Table 4. These values decrease in the order R = F_4, CF_3, F_2, F_1, and H which is in good agreement with the weakening of acceptor strength of the 3CNQ moiety, and reach to 0.5 for R = Me. The smaller $h\nu_{CT}$ values (Figure 10 and Table 4) of R = $(MeO)_2$ and $(EtO)_2$ derivatives than those of R = Me indicate that these derivatives have smaller δ_{solv} values than 0.5 in the solution state; however, these values are 0.5 and constant. A reasonable explanation of this behavior is not given at present, and the estimation of δ_{solv} value might remain somewhat ambiguous for the $\delta <$ 0.5 derivatives. Although the δ_{solv} values of R = $(MeO)_2$ and $(EtO)_2$ derivatives were estimated as nearly 0.5, the slopes a of the plots of $h\nu_{CT}$(2nd) of these derivatives vs. E_T values (Figure 12) are small negative values, implying that they have neutral ground states ($\delta_{solv} < 0.5$) in the solution state. Similar to the estimation of the δ value in the solid state, comparing the $n = 1$ ($\delta_{solv} = 0.61$) and 6 ($\delta_{solv} = 0.54$) compounds for $\mathbf{I}_n$–3CNQ-CF_3, the increase of alkyl chain length reduced the δ_{solv} value. It is plausible that the steric repulsion between the *N*-alkyl chain and the CN1 group increases with alkyl chain length (Scheme 2), and the Type II conformation, which leads to a smaller δ_{solv} value, is also preferable in the solution state.[43]

Figure 13 plots the $h\nu_{CT}$ values of $\mathbf{I}_1$–3CNQ-R (R = F_2, H, and $(EtO)_2$) against E_T values of various solvents including less-polar solvents (1,4-dioxane, PhH, PhMe, and CS_2). The plots of $\mathbf{I}_1$–3CNQ derivatives have positive slopes ($a > 0$) in solvents having higher polarity than PhCl (**a**–**d**), while the $h\nu_{CT}$ values in solvents less polar than 1,4-dioxane (**e**–**h**) were larger than that in PhCl (**d**) and showed a reverse solvato-

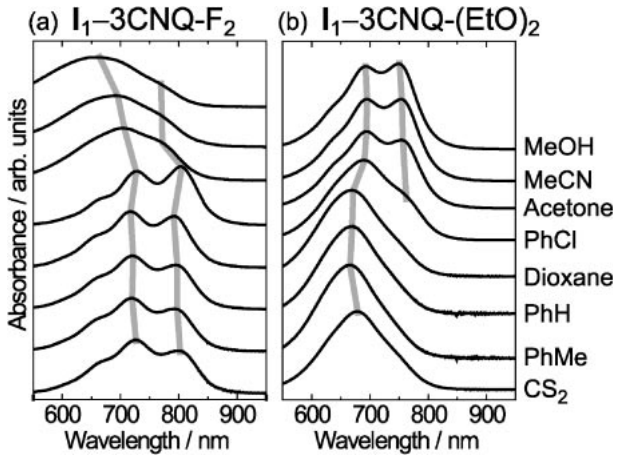

Figure 11. UV–vis spectra of (a) $\mathbf{I}_1$–3CNQ-F_2 and (b) $\mathbf{I}_1$–3CNQ-$(EtO)_2$ in MeOH, MeCN, acetone, PhCl, 1,4-dioxane, benzene (PhH), toluene (PhMe), and carbon disulfide (CS_2). Gray lines show the shifts of absorption peaks.

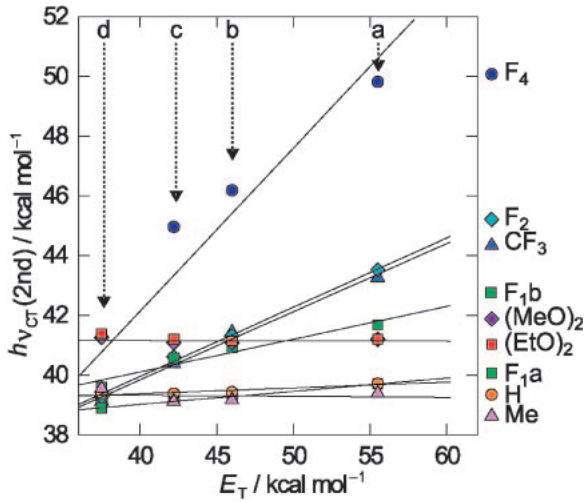

Figure 12. Plot of the $h\nu_{CT}$(2nd) values of $\mathbf{I}_1$–3CNQ-R vs. Reichardt's E_T values[5b] in various solvents. R = F_4 (blue circle), CF_3 (blue triangle), F_2 (light blue diamond), F_1a and F_1b (green squares), H (orange circle), Me (light red triangle), $(MeO)_2$ (purple diamond), and $(EtO)_2$ (red square). Solvents, **a**; MeOH ($E_T = 55.5$), **b**; MeCN (46.0), **c**; acetone (42.2), and **d**; PhCl (37.5). Lines are the least-squares fittings of each plot.

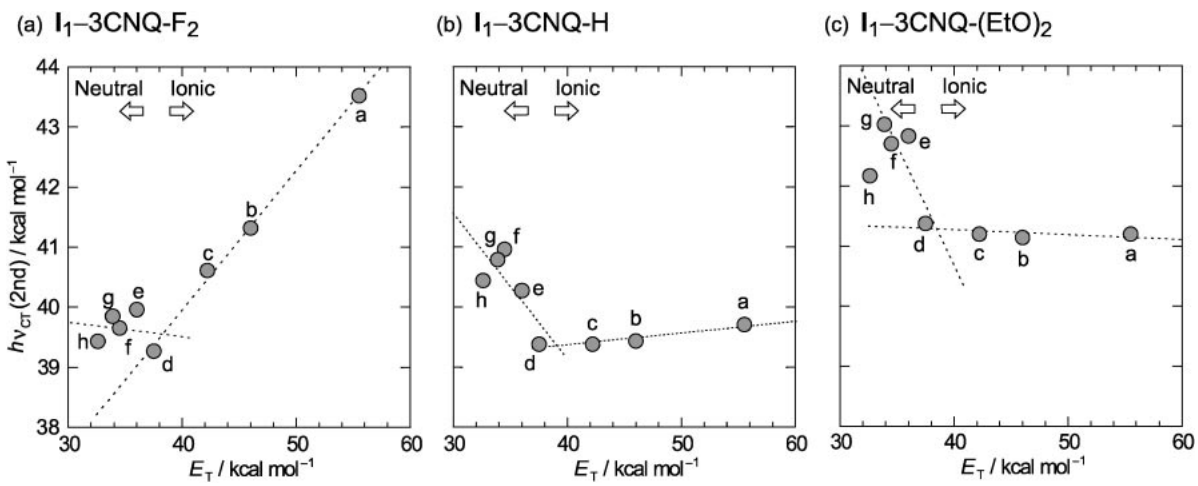

Figure 13. Plots of $h\nu_{CT}$(2nd) values of $\mathbf{I}_1$–3CNQ-R vs. Reichardt's E_T values in various solvents for (a) $\mathbf{I}_1$–3CNQ-F_2, (b) $\mathbf{I}_1$–3CNQ-H, and (c) $\mathbf{I}_1$–3CNQ-$(EtO)_2$. Solvents: **a**, MeOH ($E_T = 55.5$); **b**, MeCN (46.0); **c**, acetone (42.2); **d**, PhCl (37.5); **e**, 1,4-dioxane (36.0); **f**, PhH (34.5); **g**, PhMe (33.9); and **h**, CS_2 (32.6).

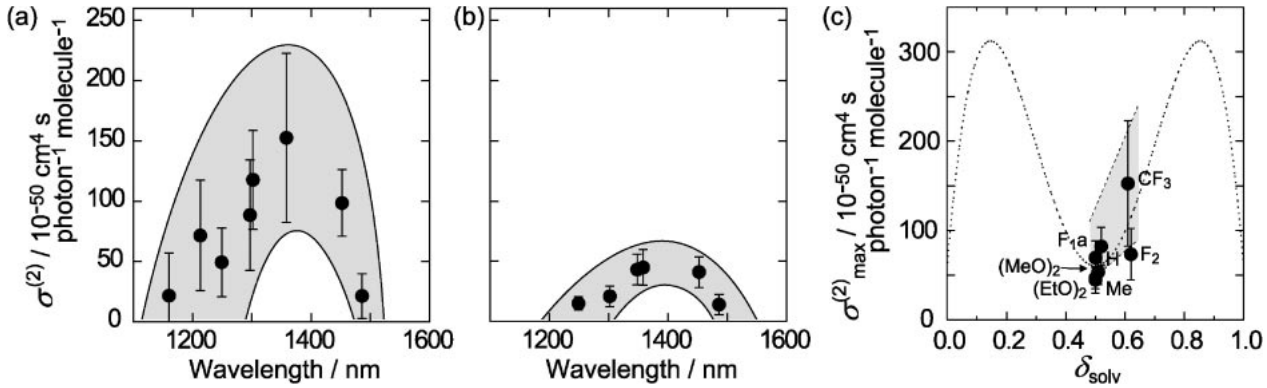

Figure 14. Two-photon absorption spectra of (a) $\mathbf{I}_1$–3CNQ-CF_3 in MeCN and (b) $\mathbf{I}_1$–3CNQ-$(EtO)_2$ in $CHCl_3$. Shaded zones cover the wavelength dependence of $\sigma^{(2)}$. (c) Plot of $\sigma^{(2)}{}_{max}$ vs. δ_{solv} of $\mathbf{I}_1$–3CNQ-R derivatives. Vertical lines are the error bars, and the shaded zone covers the wavelength and δ dependences of $\sigma^{(2)}{}_{max}$. The dotted line in (c) represents the modified eq 16 ($\sigma^{(2)}{}_{max} = 4.03 \times 10^3\delta(1-\delta)(1-2\delta)^2 + 60.3$).

Table 5. Two-Photon Absorption Properties of $\mathbf{I}_1$–3CNQ-R

Compounds	δ_{solv}	ε_{ph}/L mol^{-1} cm^{-1}	$\lambda^{(1)}_{max}$/nm	$\sigma^{(2)}_{max}$/10^{-50} cm^4 s photon^{-1} molecule^{-1}	$\lambda^{(2)}_{max}$/nm
$\mathbf{I}_1$–3CNQ-CF_3[a)]	0.61	2.36×10^4	691	152	1358
$\mathbf{I}_1$–3CNQ-F_2[a)]	0.62	3.73×10^4	692	76	1348
$\mathbf{I}_1$–3CNQ-F_1a[a),c)]	0.52	7.07×10^4	729	82	1455
$\mathbf{I}_1$–3CNQ-H[b)]	0.51	7.09×10^4	724	54	1455
$\mathbf{I}_1$–3CNQ-Me[b)]	0.50	4.73×10^4	725	47	1455
$\mathbf{I}_1$–3CNQ-$(MeO)_2$[b)]	0.50	4.58×10^4	695	70	1406
$\mathbf{I}_1$–3CNQ-$(EtO)_2$[b)]	0.50	6.38×10^4	693	45	1400

a) Measured in MeCN solution. b) Measured in $CHCl_3$ solution. c) $\mathbf{I}_1$–3CNQ-F_1a used for the two-photon absorption measurement contained several percent of $\mathbf{I}_1$–3CNQ-F_1b as minor impurity.

chromism. According to eqs 13 and 14, the $h\nu_{CT}$ values of an $\mathbf{I}_1$–3CNQ-R derivative show a linear relationship with E_T values with a positive slope ($a \geq 0$) for an ionic molecule ($0.5 \leq \delta \leq 1$), and a negative slope ($a \leq 0$) for a neutral molecule ($0 \leq \delta \leq 0.5$). Therefore, this result indicates that the ground state of $\mathbf{I}_1$–3CNQ-R changes from ionic in polar solvents ($\delta \geq 0.5$) to neutral in less-polar solvents ($\delta \leq 0.5$). Similar reverse solvatochromism in less-polar solvents has also been observed for D–3CNQ-R type $D^{\delta+}$–π–$A^{\delta-}$ [6] and phenoxide–pyridinium derivatives.[60]

(D) Two-Photon Absorption and Degree of Intramolecular CT: The two-photon absorption phenomenon of an organic chromophore, a third-order non-linear optical effect, has been attracting much interest from the viewpoints of three-dimensional microfabrication, optical data storage, optical limiting, and biological caging.[61,62] The two-photon absorption cross-section ($\sigma^{(2)}$) is proportional to the imaginary part of γ.[63] Parameters that enhance the third-order optical non-linearity are the increase in conjugation length, donor and acceptor strengths of a $D^{\delta+}$–π–$A^{\delta-}$ compound, and charge defects.[64,65]

Two-photon absorption was measured by the *Z*-scan technique at wavelengths where all compounds are non-resonant for the linear absorption.[45] Figures 14a and 14b show the relationships between $\sigma^{(2)}$ and wavelength for $\mathbf{I}_1$–3CNQ-CF_3 in MeCN and $\mathbf{I}_1$–3CNQ-$(EtO)_2$ in $CHCl_3$. The positions of one- ($\lambda^{(1)}{}_{max}$) and two-photon absorption maxima ($\lambda^{(2)}{}_{max}$) and the two-photon absorption coefficient (ε_{ph}) are summarized in Table 5. Because of the low solubility, reliable data for $\mathbf{I}_1$–3CNQ-F_4 was not obtained, and thus, not included in Table 5.

According to Kogej et al.,[21] the imaginary part of γ is attributed mainly to the dipolar term ($\approx \mu_{eg}{}^2(\mu_e - \mu_g)^2/E_{eg}{}^3$) in addition to the two-photon term ($\approx \sum \mu_{eg}{}^2\mu_{e'e}{}^2/E_{eg}{}^2E_{e'e}$), which involves the two-photon excited states denoted as e′ (eq 9). In measurements of $\mathbf{I}_1$–3CNQ-R, although the results showed a large deviation, the $\lambda^{(2)}{}_{max}$ value is close to twice the value of $\lambda^{(1)}{}_{max}$, and the dependence of $\lambda^{(2)}{}_{max}$ against the δ_{solv} value looks similar to that of $\lambda^{(1)}{}_{max}$; $\lambda^{(2)}{}_{max}$ increases with acceptor strength of the 3CNQ-R moiety from R = CF_3 to Me and then shows a blue shift for R = $(EtO)_2$ (Table 5). These observations indicate that the one- and two-photon absorption processes have the same excited state. Therefore, we hypothesized that the main contribution to $\sigma^{(2)}$ for non-centrosymmetric $\mathbf{I}_1$–3CNQ-R compounds is the dipolar term, and thus, the maximum $\sigma^{(2)}$ ($\sigma^{(2)}{}_{max}$) is approximated by eq 15,[66]

$$\sigma^{(2)}_{max} = \frac{16\pi^2}{5\hbar c^2 n^2}\frac{\mu_{eg}^2(\mu_e - \mu_g)^2}{\Gamma_{eg}} \propto \frac{\mu_{eg}^2(\mu_e - \mu_g)^2}{\Gamma_{eg}}, \qquad (15)$$

where c, n, and Γ_{eg} are the velocity of light, the refractive index of the medium, and the damping constant, respectively. Assuming Γ_{eg} does not depend on the δ value, the $\sigma^{(2)}{}_{max}$ value is expressed by δ as

$$\sigma^{(2)}{}_{max} \propto \mu_{eg}{}^2(\mu_e - \mu_g)^2 \propto \delta(1-\delta)(1-2\delta)^2, \qquad (16)$$

which shows a similar δ dependence to that of β. Accordingly, the $\sigma^{(2)}{}_{max}$ value is proportional to the product of squares of

the transition dipole moment (μ_{eg}) and the difference of dipole moments in the excited ($\mu_e = (1-\delta)ed$) and ground ($\mu_g = \delta ed$) states. In the $\delta = 0$ state, the HOMO (highest occupied molecular orbital) and LUMO (lowest unoccupied molecular orbital) of a $D^{\delta+}$–π–$A^{\delta-}$ molecule are allocated at the D and A moieties, respectively, while those of a $D^{\delta+}$–π–$A^{\delta-}$ molecule in the $\delta = 1$ state are allocated at the A and D moieties, respectively. Therefore, the δ values close to 0 and 1 result in the decrease in the overlap integral between HOMO and LUMO, leading to a small μ_{eg} value. The charge distribution of a $D^{\delta+}$–π–$A^{\delta-}$ molecule in the ground state changes to $D^{(1-\delta)+}$–π–$A^{(1-\delta)-}$ in the excited state. The μ_g and μ_e values of a $\delta = 0.5$ molecule are close to each other ($\mu_g = \mu_e = 0.5ed$), and the $|\mu_e - \mu_g|$ value ($=|(1-2\delta)ed|$) has a minimum at $\delta = 0.5$. Accordingly, eq 16 indicates that completely neutral ($\delta = 0$) and ionic ($\delta = 1$) states as well as charge delocalized state ($\delta = 0.5$) are not favorable for the $\sigma^{(2)}{}_{max}$ value, and the partially ionized state with a moderately small or large δ value is necessary to obtain a large $\sigma^{(2)}{}_{max}$ value. From eq 16, $\sigma^{(2)}{}_{max}$ exhibits maxima at $\delta = \approx 0.15$ and 0.85 and minima at $\delta = 0$, 0.5, and 1 (Figure 14c).

The magnitude of $\sigma^{(2)}$ was the largest for $\mathbf{I}_1$–3CNQ-CF_3, which has a large δ_{solv} value; whereas that of $\mathbf{I}_1$–3CNQ-$(EtO)_2$, which has the smallest δ_{solv} value, was the smallest observed thus far (Figures 14a and 14b). A rough tendency that the $\sigma^{(2)}$ value increases with the δ_{solv} value of $\mathbf{I}_1$–3CNQ-R is in agreement with the theoretical curve expected from eq 16 (Figure 14c).

Conclusion

A series of $D^{\delta+}$–π–$A^{\delta-}$ compounds ($\mathbf{I}_1$–3CNQ-R) were prepared by a Stork-enamine reaction between 1,3,3-trimethyl-2-methyleneindoline and R-TCNQ, and their structural, optical, and non-linear optical properties were investigated focusing on the degree of intramolecular CT (δ).

Structural analyses disclosed that $\mathbf{I}_1$–3CNQ-R molecules form face-to-face stacking structures in a head-to-tail manner to cancel the molecular dipole moments, and construct one-dimensional segregated or mixed stacking columnar structures of the D and A parts. Bond length ratio (*BLR*) analysis provided a qualitative estimation of the δ value in the solid state. The *BLR* values showed a good relationship with the electron-rich/deficient abilities of substituent groups and significant dependence on molecular conformation and planarity. Molecular (hyper)polarizabilities (α, β, and γ) evaluated by the MO calculation varied with the δ_{dipole} values, where their relationships with the δ values followed the theoretical curves. Optical properties of $\mathbf{I}_1$–3CNQ-R derivatives in the solution state showed significant dependences on substituent groups of the 3CNQ moiety, where the intramolecular CT band showed blue shifts with strengthening of the electron-withdrawing ability of 3CNQ-R moiety from R = Me to R = F_4 and also weakening it from R = Me to R = $(MeO)_2$ and $(EtO)_2$. $\mathbf{I}_1$–3CNQ-R derivatives also exhibited a solvatochromic shift, and the intramolecular CT bands showed a blue shift with increasing solvent polarity. Solvatochromism helped in deducing the δ_{solv} values in the solution state which increased with the electron-withdrawing ability of 3CNQ-R moieties. In the two-photon absorption measurement, the δ_{solv} value affected the two-photon cross-section ($\sigma^{(2)}$), and $\mathbf{I}_1$–3CNQ-CF_3 having the largest δ_{solv} value in the present measurements exhibited a relatively high $\sigma^{(2)}$ value.

Our investigation showed that (1) the δ values of $\mathbf{I}_1$–3CNQ-R derivatives in the solid and solution states can be controlled by chemical modification; (2) molecular (hyper)polarizabilities, which are the key parameters of non-linear optical properties, can be tuned and enhanced by controlling the δ values; and (3) the two-photon absorption properties show significant dependence on the δ values. We emphasize that our research has derived the basic and intriguing parameters of a $D^{\delta+}$–π–$A^{\delta-}$ system, which is a potential system for non-linear optical materials and will provide a new strategy in material design for the future development of $D^{\delta+}$–π–$A^{\delta-}$ based organic functional materials.

This work was partly supported by a Grant-in-Aid (21st Century COE programs on Kyoto University Alliance for Chemistry and 15205019) from the Ministry of Education, Culture, Sports, Science and Technology, Japan. T. M. is a recipient of a Japan Society for the Promotion of Science (JSPS) research fellowship.

Supporting Information

Selected physical data, crystallographic data, UV–vis, and two-photon absorption measurements for $\mathbf{I}_n$–3CNQ-R. This material is available free of charge at http://www.csj.jp/journals/bcsj/.

References

1 Preliminary accounts of a part of this work: a) C.-H. Chong, M. Makihara, G. Saito, *Mol. Cryst. Liq. Cryst.* **2002**, *376*, 183. b) G. Saito, C.-H. Chong, M. Makihara, A. Otsuka, H. Yamochi, *J. Am. Chem. Soc.* **2003**, *125*, 1134.

2 A. Aviram, M. A. Ratner, *Chem. Phys. Lett.* **1974**, *29*, 277.

3 Reviews for unimolecular D–A systems: a) G. Ho, J. R. Heath, M. Kondratenko, D. F. Perepichka, K. Arseneault, M. Pézolet, M. R. Bryce, *Chem.—Eur. J.* **2005**, *11*, 2914. b) M. Bendikov, F. Wudl, D. F. Perepichka, *Chem. Rev.* **2004**, *104*, 4891.

4 Comprehensive reviews for unimolecular rectifiers based on D–3CNQ molecules: a) R. M. Metzger, *Acc. Chem. Res.* **1999**, *32*, 950. b) R. M. Metzger, *J. Mater. Chem.* **1999**, *9*, 2027. c) R. M. Metzger, *Chem. Rev.* **2003**, *103*, 3803. d) R. M. Metzger, *Anal. Chim. Acta* **2006**, *568*, 146.

5 a) C. Reichardt, *Angew. Chem., Int. Ed. Engl.* **1965**, *4*, 29. b) C. Reichardt, *Chem. Rev.* **1994**, *94*, 2319.

6 N. A. Bell, D. J. Crouch, D. J. Simmonds, A. E. Goeta, T. Gelbrich, M. B. Hursthouse, *J. Mater. Chem.* **2002**, *12*, 1274.

7 R. M. Metzger, N. E. Heimer, G. J. Ashwell, *Mol. Cryst. Liq. Cryst.* **1984**, *107*, 133.

8 R. M. Metzger, B. Chen, U. Höpfner, M. V. Lakshmikantham, D. Vuillaume, T. Kawai, X. Wu, H. Tachibana, T. V. Hughes, H. Sakurai, J. W. Baldwin, C. Hosch, M. P. Cava, L. Brehmer, G. J. Ashwell, *J. Am. Chem. Soc.* **1997**, *119*, 10455.

9 A. Honciuc, A. Otsuka, Y.-H. Wang, S. K. McElwee, S. A. Woski, G. Saito, R. M. Metzger, *J. Phys. Chem. B* **2006**, *110*, 15085.

10 G. J. Ashwell, W. D. Tyrrell, A. J. Whittam, *J. Am. Chem. Soc.* **2004**, *126*, 7102.

11 G. Wen, Y. Wang, Y. Song, Z. Lu, D. Zhang, Y. Liu, D.

Zhu, *Chem. Phys. Lett.* **2006**, *431*, 370.
12 G. J. Ashwell, *Thin Solid Films* **1990**, *186*, 155.
13 A. M. R. Beaudin, N. Song, Y. Bai, L. Men, J. P. Gao, Z. Y. Wang, M. Szablewski, G. Cross, W. Wenseleers, J. Campo, E. Goovaerts, *Chem. Mater.* **2006**, *18*, 1079.
14 M. Szablewski, P. R. Thomas, A. Thornton, D. Bloor, G. H. Cross, J. M. Cole, J. A. K. Howard, M. Malagoli, F. Meyers, J.-L. Brédas, W. Wenseleers, E. Goovaerts, *J. Am. Chem. Soc.* **1997**, *119*, 3144.
15 a) S. R. Marder, C. B. Gorman, B. G. Tiemann, J. W. Perry, G. Bourhill, K. Mansour, *Science* **1993**, *261*, 186. b) S. R. Marder, C. B. Gorman, F. Meyers, J. W. Perry, G. Bourhill, J.-L. Brédas, B. M. Pierce, *Science* **1994**, *265*, 632. c) F. Meyers, S. R. Marder, B. M. Pierce, J.-L. Brédas, *J. Am. Chem. Soc.* **1994**, *116*, 10703.
16 M. Barzoukas, C. Runser, A. Fort, M. Blanchard-Desce, *Chem. Phys. Lett.* **1996**, *257*, 531.
17 D. J. Williams, *Angew. Chem., Int. Ed. Engl.* **1984**, *23*, 690.
18 H. E. Katz, K. D. Singer, J. E. Sohn, C. W. Dirk, L. A. King, H. M. Gordon, *J. Am. Chem. Soc.* **1987**, *109*, 6561.
19 a) J. Garín, J. Orduna, J. I. Rupérez, R. Alcalá, B. Villacampa, C. Sánchez, N. Martín, J. L. Segura, M. González, *Tetrahedron Lett.* **1998**, *39*, 3577. b) M. R. Bryce, A. Green, A. J. Moore, D. F. Perepichka, A. S. Batsanov, J. A. K. Howard, I. Ledoux-Rak, M. González, N. Martín, J. L. Segura, J. Garín, J. Orduna, R. Alcalá, B. Villacampa, *Eur. J. Org. Chem.* **2001**, 1927.
20 S. Alías, R. Andreu, M. A. Cerdán, S. Franco, J. Garín, J. Orduna, P. Romero, B. Villacampa, *Tetrahedron Lett.* **2007**, *48*, 6539.
21 a) T. Kogej, D. Beljonne, F. Meyers, J. W. Perry, S. R. Marder, J. L. Brédas, *Chem. Phys. Lett.* **1998**, *298*, 1. b) D. Beljonne, T. Kogej, S. R. Marder, J. W. Perry, J. L. Brédas, *Mol. Cryst. Liq. Cryst. Sci. Technol., Sect. B* **1999**, *21*, 461.
22 J. C. May, I. Biaggio, F. Bures, F. Diederich, *Appl. Phys. Lett.* **2007**, *90*, 251106.
23 H. Kang, A. Facchetti, H. Jiang, E. Cariati, S. Righetto, R. Ugo, C. Zuccaccia, A. Macchioni, C. L. Stern, Z. Liu, S.-T. Ho, E. C. Brown, M. A. Ratner, T. J. Marks, *J. Am. Chem. Soc.* **2007**, *129*, 3267.
24 a) K. Higashino, T. Nakaya, E. Ishiguro, *J. Photochem. Photobiol., A* **1994**, *79*, 81. b) R. M. Williams, J. M. Zwier, J. W. Verhoeven, *J. Am. Chem. Soc.* **1995**, *117*, 4093. c) S. Kim, H. Choi, C. Baik, K. Song, S. O. Kang, J. Ko, *Tetrahedron* **2007**, *63*, 11436.
25 a) G. J. Ashwell, E. J. C. Dawnay, A. P. Kuczynski, M. Szablewski, I. M. Sandy, M. R. Bryce, A. M. Grainger, M. Hasan, *J. Chem. Soc., Faraday Trans.* **1990**, *86*, 1117. b) Y. Onganer, M. Yin, D. R. Bessire, E. L. Quitevis, *J. Phys. Chem.* **1993**, *97*, 2344.
26 a) Y. Tsubata, T. Suzuki, T. Miyashi, Y. Yamashita, *J. Org. Chem.* **1992**, *57*, 6749. b) T. Suzuki, S. Miyanari, Y. Tsubata, T. Fukushima, T. Miyashi, Y. Yamashita, K. Imaeda, T. Ishida, T. Nogami, *J. Org. Chem.* **2001**, *66*, 216. c) T. Suzuki, M. Yamada, M. Ohkita, T. Tsuji, *Heterocycles* **2001**, *54*, 387. d) T. Suzuki, S. Miyanari, H. Kawai, K. Fujiwara, T. Fukushima, T. Miyashi, Y. Yamashita, *Tetrahedron* **2004**, *60*, 1997.
27 a) O. Neilands, V. Tilika, I. Sudmale, I. Grigorjeva, A. Edzina, E. Fonavs, I. Muzikante, *Adv. Mater. Opt. Electron.* **1997**, *7*, 39. b) O. Neilands, *Mol. Cryst. Liq. Cryst.* **2001**, *335*, 331. c) K. Balodis, S. Khasanov, C. Chong, M. Maesato, H. Yamochi, G. Saito, O. Neilands, *Synth. Met.* **2003**, *133–134*, 353.
28 S. Nishida, Y. Morita, K. Fukui, K. Sato, D. Shiomi, T. Takui, K. Nakasuji, *Angew. Chem., Int. Ed.* **2005**, *44*, 7277.
29 A. J. Banister, N. Bricklebank, I. Lavender, J. M. Rawson, C. I. Gregory, B. K. Tanner, W. Clegg, M. R. J. Elsegood, F. Palacio, *Angew. Chem., Int. Ed. Engl.* **1996**, *35*, 2533.
30 M. Szablewski, *J. Org. Chem.* **1994**, *59*, 954.
31 a) B. C. McKusick, R. E. Heckert, T. L. Cairns, D. D. Coffman, H. F. Mower, *J. Am. Chem. Soc.* **1958**, *80*, 2806. b) P. G. Farrell, R. K. Wojtowski, *J. Chem. Soc. C* **1970**, 1390.
32 Z. Rappoport, A. Horowitz, *J. Chem. Soc.* **1964**, 1348.
33 T. Ishiguro, K. Yamaji, G. Saito, *Organic Superconductors*, 2nd ed., Springer-Verlag, Berlin, **1998**.
34 G. Saito, J. P. Ferraris, *Bull. Chem. Soc. Jpn.* **1980**, *53*, 2141.
35 J. B. Torrance, *Acc. Chem. Res.* **1979**, *12*, 79.
36 a) J. B. Torrance, J. E. Vazquez, J. J. Mayerle, V. Y. Lee, *Phys. Rev. Lett.* **1981**, *46*, 253. b) S. Horiuchi, R. Kumai, Y. Okimoto, Y. Tokura, *Chem. Phys.* **2006**, *325*, 78.
37 H. M. McConnell, B. M. Hoffman, R. M. Metzger, *Proc. Natl. Acad. Sci. U.S.A.* **1965**, *53*, 46.
38 H. Seo, *J. Phys. Soc. Jpn.* **2000**, *69*, 805.
39 A. Broo, M. C. Zerner, *Chem. Phys.* **1995**, *196*, 407.
40 J. Catalán, E. Mena, W. Meutermans, J. Elguero, *J. Phys. Chem.* **1992**, *96*, 3615.
41 A. Broo, M. C. Zerner, *Chem. Phys.* **1995**, *196*, 423.
42 E. Alcalde, I. Dinarés, J. Elguero, J.-P. Fayet, M.-C. Vertut, C. Miravitlles, E. Molins, *J. Org. Chem.* **1987**, *52*, 5009.
43 T. Murata, K. Nishimura, Y. Enomoto, G. Honda, Y. Shimizu, A. Otsuka, G. Saito, *Bull. Chem. Soc. Jpn.* **2008**, *81*, 869.
44 Y. Ogata, J. Kawamata, C.-H. Chong, A. Yamagishi, G. Saito, *Clays Clay Miner.* **2003**, *51*, 181.
45 M. Sheik-Bahae, A. A. Said, T.-H. Wei, D. J. Hagan, E. W. van Stryland, *IEEE J. Quantum Electron.* **1990**, *26*, 760.
46 R. L. Sutherland, *Handbook of Nonlinear Optics*, Marcel Dekker, New York, **1996**.
47 a) R. R. Tykwinski, K. Kamada, D. Bykowski, F. A. Hegmann, R. J. Hinkle, *J. Opt. A: Pure Appl. Opt.* **2002**, *4*, S202. b) K. Kamada, K. Ohta, Y. Iwase, K. Kondo, *Chem. Phys. Lett.* **2003**, *372*, 386.
48 G. M. Sheldrick, *Program for the Solution of Crystal Structuers*, University of Göttingen, Göttingen, Germany, **1997**.
49 G. M. Sheldrick, *Program for the Refinement of Crystal Structures*, University of Göttingen, Göttingen, Germany, **1997**.
50 N. A. Bell, C. S. Bradley, R. A. Broughton, S. J. Coles, D. E. Hibbs, M. B. Hursthouse, A. K. Ray, D. J. Simmonds, S. C. Thorpe, *J. Mater. Chem.* **2005**, *15*, 1437.
51 M. Pickholz, M. C. dos Santos, *THEOCHEM* **1998**, *432*, 89.
52 R. S. Mulliken, *J. Am. Chem. Soc.* **1952**, *74*, 811.
53 J. Ducuing, C. Flytzanis, in *Optical Properties of Solids*, ed. by F. Abelès, North-Holland Pub. Co., Amsterdam, **1972**.
54 R. Foster, *Organic Charge-Transfer Complexes*, Academic Press, New York, **1969**.
55 I. Gruda, F. Bolduc, *J. Org. Chem.* **1984**, *49*, 3300.
56 Y. Hirano, J. Kawata, Y. F. Miura, M. Sugi, T. Ishii, *Thin Solid Films* **1998**, *327–329*, 345.
57 S. A. Krysanov, M. V. Alfimov, *Chem. Phys. Lett.* **1981**, *82*, 51.
58 E. M. Kosower, *J. Am. Chem. Soc.* **1958**, *80*, 3261.
59 J. W. Baldwin, B. Chen, S. C. Street, V. V. Konovalov, H. Sakurai, T. V. Hughes, C. S. Simpson, M. V. Lakshmikantham, M. P. Cava, L. D. Kispert, R. M. Metzger, *J. Phys. Chem. B* **1999**, *103*, 4269.

60 a) C. Machado, M. G. Nascimento, M. C. Rezende, *J. Chem. Soc., Perkin Trans. 2* **1994**, 2539. b) C. Runser, A. Fort, M. Barzoukas, C. Combellas, C. Suba, A. Thiébault, R. Graff, J. P. Kintzinger, *Chem. Phys.* **1995**, *193*, 309.

61 J. D. Bhawalkar, G. S. He, P. N. Prasad, *Rep. Prog. Phys.* **1996**, *59*, 1041.

62 R. H. Köhler, J. Cao, W. R. Zipfel, W. W. Webb, M. R. Hanson, *Science* **1997**, *276*, 2039.

63 M. Albota, D. Beljonne, J.-L. Brédas, J. E. Ehrlich, J.-Y. Fu, A. A. Heikal, S. E. Hess, T. Kogej, M. D. Levin, S. R. Marder, D. McCord-Maughon, J. W. Perry, H. Röckel, M. Rumi, G. Subramaniam, W. W. Webb, X.-L. Wu, C. Xu, *Science* **1998**, *281*, 1653.

64 See for example: *Nonlinear Optical Properties of Organic Molecules and Crystals*, ed. by D. S. Chemla, J. Zyss, Academic Press, Orlando, **1987**.

65 H. Fujita, M. Nakano, M. Takahata, K. Yamaguchi, *Chem. Phys. Lett.* **2002**, *358*, 435.

66 K. Ohta, L. Antonov, S. Yamada, K. Kamada, *J. Chem. Phys.* **2007**, *127*, 084504.